Bio-based, internally pH sensitive materials: immobilized yellow fluorescent protein as optical sensor for spatiotemporal mapping of pH inside porous matrices

*Tanja Consolati[1], Juan M. Bolivar[1], Zdenek Petrasek[1], Jose Berenguer[2], Aurelio Hidalgo[2], Jose M. Guisán[3] and Bernd Nidetzky[1,4]**

[1] Institute of Biotechnology and Biochemical Engineering, Graz University of Technology, NAWI Graz, Petersgasse 12, A-8010 Graz, Austria

[2] Department of Molecular Biology, Universidad Autónoma de Madrid, Center for Molecular Biology 'Severo-Ochoa' (UAM-CSIC), Nicolás Cabrera 1, Madrid, Spain

[3] Institute of Catalysis and Petroleum Chemistry (ICP-CSIC), C/ Marie Curie, 2, Cantoblanco 28049, Madrid, Spain

[4] Austrian Centre of Industrial Biotechnology, Petersgasse 14, A-8010 Graz, Austria

E-mail: bernd.nidetzky@tugraz.at

Keywords: porous materials, internal pH sensing, yellow fluorescent protein, immobilization, spatiotemporal pH mapping

ABSTRACT

The pH is fundamental to biological function and its measurement therefore crucial across all biosciences. Unlike homogenous bulk solution, solids often feature internal pH gradients due to partition effects and confined biochemical reactions. Thus, a full spatiotemporal mapping for pH characterization in solid materials with biological systems embedded in them is essential. In here, therefore, a fully biocompatible methodology for real-time optical sensing of pH within porous materials is presented. A genetically encoded ratiometric pH sensor, the enhanced superfolder yellow fluorescent protein (sYFP), is used to functionalize the internal surface of different materials, including natural and synthetic organic polymers as well as silica frameworks. By using controlled, tailor-made immobilization, sYFP is homogeneously distributed within these materials, and so enables, via self-referenced imaging analysis, pH measurements in high accuracy and with useful spatiotemporal resolution. Evolution of internal pH is monitored in consequence of a proton-releasing enzymatic reaction, the hydrolysis of penicillin by a penicillin acylase, taking place in solution or confined to the solid surface of the porous matrix. Unlike opto-chemical pH sensors, which often interfere with biological function, labeling with sYFP enables pH sensing without altering the immobilized enzyme's properties in any of the materials used. Fast response of sYFP to pH change permits evaluation of biochemical kinetics within the solid materials. Thus, pH sensing based on immobilized sYFP represents a broadly applicable technique to the study of biology confined to the internally heterogeneous environment of solid matrices.

1. INTRODUCTION

Although often studied in conditions of ideal mixtures, most of natural biology happens in heterogeneous environments.[1–5] Solid matrices, and interfacial phenomena at their surfaces, are prevalent in biological systems and have a formative influence on them.[1,2,6–8] In mimicking the structure and function of these matrices, and by extending their properties beyond natural limits, modern functional materials play an instrumental role in advancing biology.[9–14] These materials enable systems characterization to fully embrace the complex effect of physico-chemical heterogeneity. They are vital to the engineering of biology for diverse applications in biotechnology, biomedicine and bioanalytics.[11,13–19] However, ability to observe and control the microenvironment of the solid matrix is essential to the study, and the qualified use, of the biology confined within.[18,20–22] Parameter of paramount importance for proper biological function, and hence for measurement in all of the experimental biosciences, is the proton concentration, the pH.[23,24]

While it can be measured conveniently in bulk solution, the pH within a porous matrix, and at liquid-solid interface, is difficult to access. Knowing the pH conditions under interfacial confinement is however very important, for they may differ substantially from the one prevailing in bulk solution due to effects of interphase thermodynamics and diffusion combined.[20,21,25,26] Whenever a biochemical reaction involves the proton directly, the "pH confined" exhibits pronounced spatiotemporal variation and so may deviate from the bulk pH to a large extent.[27–32] Despite previous efforts, complex aspects of pH analytics, including instrumental set-up, spatiotemporal resolution and method invasiveness, mean that pH measurement within porous matrices remains a largely unsolved problem.[20,21]

Opto-chemical sensing appears particularly apt to the monitoring of pH in complex biological environments.[33,34] Its basic principle involves a fluorescent pH indicator embedded within an analyte-permeable polymeric layer. This is further system-integrated by controlled deposition as in sensor spots and optical fiber tips, enabling different and often contactless optical readouts.[33,34] Its widespread applicability in biological studies notwithstanding, the methodology in the current form cannot be used to analyze the pH within solid porous materials. Alternatively, labeling with a pH indicator luminescence dye is useful to render the porous material internally pH-sensitive. Grafting the dye on the surface, or incorporating it directly into the matrix material, are known ways of luminescence labeling in principle.[20,21,27,29,31,32,35,36] However, the development of a suitable labeling procedure is always case-specific. Problems associated with common luminescence dyes (e.g., fluorescein) include low biocompatibility, low photostability and an insufficient pH range. They also often lack the possibility of self-referenced measurement,[20,21] which makes additional labeling of the material with a pH-independent luminescence dye necessary, thus further complicating the whole system. Lastly, the spatiotemporal resolution of pH mapping in dual-labeled materials is usually relatively low, unless highly specialized instrumentation is used.

The current study was performed with the idea of significant advance from a bio-inspired approach: fluorescent protein immobilized on the internal pore surface of solid matrices is used as a pH-sensitive nano-optode for measuring the pH confined within. The class of fluorescent proteins, most prominently represented by the green fluorescent protein from the jellyfish *Aequorea victoria*, is well known for having revolutionized the study of live cell biology.[37–40] Through molecular engineering, genetically encoded fluorescent proteins can be structurally adapted and their opto-chemical function fine-tuned.[38] More recently, their application was

expanded to different areas of biosensing, including intracellular pH,[37–42] showing a broad range of temperature and pH of stability.[37–42] Fluorescent protein-based pH indicators are categorized according to whether they enable self-referenced ratiometric measurement. Unlike sensors solely based on intensity, a ratiometric sensor exhibits pH-dependent changes of the shape of excitation or emission spectra. This makes it possible to measure fluorescence intensities in two selected wavelength ranges, and to determine pH from their ratio. Since this ratio is independent of the total fluorescence intensity, this procedure removes the intrinsic limitation of intensity-based measurement, where signal correction for optical interference from the readout system or effects of photobleaching and inhomogeneous loading of the luminescence indicator molecule are impossible. Up to now, however, there are only a few in vivo studies demonstrating ratiometric pH sensing using fluorescent proteins.[43–45]

Here, we present superfolder yellow fluorescent protein (sYFP)[46,47] as a powerful ratiometric pH indicator suitable both in solution and within porous matrices. sYFP belongs to a new generation of enhanced YFP with improved stability and folding kinetics.The sYFP is highly stable and its pH dependent fluorescence covers the relevant (neutral) pH range. [46,47] Despite detailed characterization of sYFP recent studies,[46,47] the protein's suitability as ratiometric pH sensor was not previously assessed. We also show that pH sensing using immobilized sYFP on solid surface in a tailor-made fashion is widely applicable to a broad variety of materials and well suited to the study of biology confined to these solid matrices

2. EXPERIMENTAL SECTION

2.1. Materials used

Penicillin G acylase (PGA) from *Escherichia coli* and penicillin G (PenG) were from Antibióticos S.A. (León, Spain). Agarose 6 BCL (Ag BCL) STANDARD (particle size 50-150 μm) or FINE (particle size 20-50 μm) was from Agarose Bead Technologies (Madrid, Spain). TRISOPERL® controlled pore glass (CPG) beads (particle size 50-100 μm diameter, pore size 161.2 nm, pore volume 1520.91 mm^3 g^{-1} and specific surface area 43.16 m^2 g^{-1}) were from VitraBio GmbH (Steinach, Germany). Sepabeads® EC-EP (Sep) standard grade (particle size 150-300 μm; pore size 10-20 nm) were from Resindion (Milano, Italy). Serum bovine albumin, epichlorohydrine, sodium borohydrate, 2-nitro-5-phenylacetamidobenzoic acid, (3-glycidoxypropyl) trimethoxysilane, N,N-diisopropylcarbodiimide, N-hydroxysuccinimide, ethanolamine, imidazole, iminodiacetic acid and phenyl acetic acid were from Sigma Aldrich (St Louis MO, USA). Standard chemicals and reagents were of analytical grade. Epoxy activated agarose[48], glyoxyl agarose (Ag-Gly),[49] epoxy activated CPG [50] and metal chelate supports (Ag-Ni, CPG-Ni and Sep-Ni)[48] were prepared according to reported protocols with the modifications described in the ESI.

2.2 Protein preparation

Full-length sYFP was cloned into a pET28b(+) vector to obtain a N-terminally hexahistidine-tagged protein, referred to as sYFP throughout this manuscript. Recombinant protein was expressed in *E. coli* BL21(DE3) cultured at 37 °C. Luria-Bertani Medium containing Kanamycin (50 μg mL^{-1}) was used and expression was induced with IPTG (0.5 mM) at an OD_{595} of 0.5 for 5 - 6 h. Cells resuspended in lysis buffer (10 mM sodium phosphate, pH 7.00) were sonicated (15 min, 0.6 Hz, 50% amplitude) and centrifuged (20 min, 20,000 g, 4°C). Ten mL of lysate (supplemented with 30 mM of imidazole to prevent unspecific protein adsorption) were

incubated with 1.0 g of Ag-Ni ON at 4°C. The support was washed with lysis buffer and bound sYFP was then washed off with 1 M of imidazole. The protein solution was dialyzed at 4°C overnight against 10 mM sodium phosphate buffer (pH 7.50). PGA was obtained by dialyzing *E. coli* cell extract against a 50 mM sodium phosphate buffer (pH 7.50; 4°C, overnight). For microscopy experiments, the soluble enzyme was concentrated 10-fold and buffer was exchanged to 5 mM sodium phosphate (pH 7.00) using 10 kDa MWCO Amicon Ultra centrifugal filters (Milipore, Germany). Proteins were stored at -20°C until use.

2.3 Protein immobilization

The sYFP (8-10 mg g^{-1} carrier) was immobilized on metal chelate supports and on Ag-Gly. For immobilization, 10 mL of protein solution were incubated with 1.0 g of support. To slow down the enzyme immobilization for homogeneous protein distribution on the support, a gradually decreasing concentration of a competing ligand was used. Immobilization on metal chelate supports involved buffers (25 mM sodium phosphate, pH 8.00) supplemented with 300 mM $\rightarrow$ 37.5 mM imidazole. Immobilization on Ag-Gly used buffer (100 mM sodium bicarbonate, pH 10.05) supplemented with 1 M $\rightarrow$ 31.25 mM ethanolamine. The immobilization mixture was left for 12 h at 4°C at the lowest ligand concentration. PGA (2-400 U_{NiPAB} g^{-1} carrier) was immobilized covalently on the glyoxyl groups on Ag-Ni support as reported previously[49] (see the Supporting Information for details). The PGA Ag-Ni immobilizates were washed with distilled water and Ni^{2+} was reloaded by incubation for 30 min in 10 mM sodium phosphate buffer (pH 7.00) containing $NiSO_4$ (1 mg mL^{-1}). Immobilization of sYFP was performed as described above for metal chelate supports. Incubation in $NiSO_4$ did not affect PGA activity measured with NiPAB as the substrate. The progress of immobilization was monitored from measurements of

the PGA activity towards NIPAB. The amount of protein or activity immobilized was calculated from protein mass or activity balances. Immobilization yield is defined as the percentage ratio of bound to offered protein or activity. SDS-PAGE, protein concentration determination and (free or immobilized) PGA activity assays were performed by adaptation of reported procedures (see the Supporting Information for full details).

2.4 Fluorescence spectroscopy

Excitation and emission spectra were recorded on a Hitachi (Tokyo, Japan) F4500 Spectrofluorometer. The excitation wavelength was 458 nm; the emission wavelength was 540 nm. The excitation and emission slits were set to 2.5 nm. Spectra were recorded with a wavelength step of 1 nm. All measurements were performed at room temperature. The concentration of sYFP was the same at all pH values.

2.5 Ratiometric pH-sensing analysis

Ratiometric imaging was conducted with a Zeiss LSM 710 inverted confocal microscope (Carl Zeiss, Jena, Germany) using an EC Plan-Neofluar 10X/0.30 M27 objective. For the emission ratiometric imaging (Em_r), excitation wavelength was 458 nm and emission was collected simultaneously at 515-600 nm and 475-515 nm. In the excitation ratiometric method (Ex_r), sample was excited consecutively at 488 nm and 458 nm while emission was monitored at 500-600 nm. For calibration, stock solutions of soluble sYFP, immobilized sYFP and sYFP-PGA-coimmobilizates were diluted in calibration buffer (20 mM citrate/100 mM phosphate, pH 5.00 - 10.00). Final concentrations were 1 mg mL^{-1} for soluble sYFP and 1:200 w v^{-1} particle suspension for immobilizates. About 200 µL of each sample was transferred to an 8-well µ-Slide (Ibidi, Germany) and imaged as described above. The pH of the calibration buffers was set using

a standard pH meter. For pH time courses, stock solution of sYFP and sYFP-immobilizates (pre-equilibrated in reaction buffer) were diluted in reaction buffer (10 to 200 mM sodium phosphate buffer, pH 8.00 - 9.00, as indicated for each experiment). Final concentrations were 1 mg mL^{-1} for soluble sYFP and 1:1000 w v^{-1} particle suspension for immobilizates. For experiments performed with sYFP and immobilized sYFP, PGA was added to the final concentration indicated. Experiments carried out with sYFP-PGA-coimmobilizates (i.e., catalyst particles) additionally contained so-called bulk particles. These bulk particles consisted of sYFP immobilized on Agarose 6 BCL FINE. sYFP-PGA-coimmobilizates (catalyst particles) were mixed 1:1 with bulk particles pre-equilibrated in reaction buffer and diluted to a final particle suspension of 1:1000 w v^{-1} in reaction buffer. All time courses were imaged for about 20 s before reaction was started by the addition of concentrated PenG stock solution (200-400 mM in 50 mM sodium phosphate buffer, pH 9.00) to a final concentration of 10 mM (sYFP and immobilized sYFP) or 20 mM (sYFP-PGA-coimmobilizate). Addition of PenG in the absence of PGA did not lead to a decrease in pH. A slight movement of particles due to substrate addition also did not affect the pH measurements. The reaction volume was kept constant at 200 µL in each experiment. Photobleaching was analyzed, and controlled for, by recording images from the samples over the duration of an average measurement.

For pH maps images were exported from Fiji imageJ (processing package software version ImageJ 1.49d (http://fiji.sc/Fiji)) to Matlab. The pH mapping was performed on a pixel-by-pixel basis. It involved calculating the ratio *R* between two images taken with different excitation wavelengths (the excitation ratiometric method) or recorded at different emission ranges (the emission ratiometric method). The ratio *R* was then converted to pH as described below (2.6

Analysis of the pH response). Finally, the obtained pH value in every pixel was displayed using a color defined by a color bar shown in every figure.

2.6 Analysis of the pH response

Analysis of ratiometric imaging was performed using Fiji imageJ. Region of interests (ROIs) were selected manually in each processed image. The mean intensity of the selected area was calculated for ROI and fluorescence channel. Values were exported to Sigmaplot and fluorescence intensity ratio (*R*) of the two wavelength couples chosen for Ex_r (F(488, 500-600)/F(458, 500-600)) and Em_r (F(458, 515-600)/F(458, 475-515)) was calculated.

The dependence of *R* on pH can be described by the two-state model of fluorophore protonation according to Equation 1, as suggested in literature.[44,45]

$$R = R_0 \cdot \left(\frac{R_f + 10^{(pK' - pH)}}{1 + 10^{(pK' - pH)}} \right) \qquad (1)$$

In Equation 1, R_0 (ratiometric offset) is the fluorescence ratio *R* in the limit of low pH; the product R_0R_f is the fluorescence ratio *R* in the limit of high pH; and p*K*' (ratiometric p*K*') is an effective p*K* value that depends on the intrinsic p*K* but also on the fluorescence intensities of the ratiometric probe at low and high pH (see the Supporting Information). The values R_0, R_f and pK' were obtained from fits of Equation 1 to the experimental pH dependence of *R*. The ratiometric nature of all parameters in Equation 1 makes *R* independent on fluorophore concentration, photobleaching or the optical system. The p*K*' and R_f only depend on the photophysical and thermodynamic properties of the fluorescent protein as well as on the selected wavelength pairs. R_0 is influenced by instrumental characteristics, such as the excitation intensity and the detector efficiency, as it represents a fluorescence ratio taken with two distinct excitation/emission

settings.[45] The fluorescent molecule only behaves as a ratiometric probe when $R_f \neq 1$, i.e., the fluorescence probe undergoes a different variation in optical signal between the two chosen wavelength pairs.

The pH was calculated according to Equation 2.

$$\mathrm{pH} = \mathrm{pK'} - \log_{10}\left(\frac{\frac{\mathrm{R}}{\mathrm{R}_0} - \mathrm{R}_\mathrm{f}}{1 - \frac{\mathrm{R}}{\mathrm{R}_0}}\right) \qquad (2)$$

Analysis of error propagation in pH determination and assessment of the sensitivity of the pH measurement are shown in the Supporting Information.

3. RESULTS AND DISCUSSION

3.1. sYFP as ratiometric pH indicator

We initially analyzed the pH-dependent fluorescence properties of the soluble sYFP to address the suitability of ratiometric sensing. Both the emission and the excitation spectra varied not only in intensity, as expected,[46,47] but also in shape in response to pH change (Figure S1). These distinct spectral forms variable on pH are the suggestion of different protein species with different fluorescence properties.[45] The principal component analysis (PCA) of the spectra indicated that every spectrum could be expressed as a sum of only two components, which we attributed to the protonated (low-pH) and deprotonated (high-pH) sYFP forms (Figure S1). Combining the results of PCA with the additional assumption of protonation equilibrium between the two sYFP-species ([protonated]/[deprotonated]=$10^{pK\text{-}pH}$), we calculated the shapes of the

emission and excitation spectra of the two species (Figure S1, B and D). The p*K* value of 6.98 and 6.92 was thus obtained from the emission and excitation spectra, respectively.

From the relevant spectra, therefore, we chose wavelength ranges 475-515 nm and 515-600 nm for emission ratiometric measurement to detect preferentially the protonated and deprotonated forms of sYFP. Being limited by the available lasers in the microscope, we chose for excitation ratiometric measurement 488 nm and 458 nm to excite the high-pH and the low-pH sYFP forms, respectively. By determining the fluorescence intensity ratio R (= F_1/F_2) from intensities F recorded in separate channels, we showed that R exhibited sigmoidal dependence on pH (Figure S2, Equation 1). The apparent p*K*', corresponding to the respective curve's inflection point, was obtained as 7.43 and 6.98 from, respectively, emission (Em_r) and excitation (Ex_r) ratiometric measurements, as shown in Table 1. The region of largest variation in R is therefore at pH = p*K*´ ± 1, as seen in Figure S2.

Table 1. Characterization of different sYFP-materials as ratiometric pH sensors

	Excitation			**Emission**		
	R_0	p*K*'	R_f	R_0	p*K*'	R_f
Soluble sYFP	0.11 ± 0.01	6.82 ± 0.01	14.12 ± 1.49	0.37 ± 0.10	7.43 ± 0.07	9.03 ± 2.45
Ag-Ni	0.08 ± 0.01	7.01 ± 0.03	12.3 ± 1.56	0.39 ± 0.02	7.73 ± 0.02	8.43 ± 0.33
Glyoxyl-Ag	0.22 ± 0.03	6.61 ± 0.05	4.96 ± 0.78	0.45 ± 0.05	7.31 ± 0.03	8.01 ± 0.92
CPG-Ni	0.05 ± 0.03	6.70 ± 0.07	23.52 ± 14.49	0.36 ± 0.05	7.51 ± 0.03	11.72 ± 1.49
Sep-Ni	0.07 ± 0.02	6.99 ± 0.04	17.2 ± 5.24	0.38 ± 0.04	7.69 ± 0.04	9.41 ± 1.03

Parameters are from nonlinear fits of Equation 1 to the pH response curves of soluble sYFP or sYFP attached to the solid material.

The dynamic response of the sYFP as pH sensor was assessed from the decrease in pH due to enzymatic hydrolysis of penicillin G in a homogeneous solution. As expected, the rates of pH drop were dependent on the amount of enzyme added in a roughly linear fashion (Figure S3). The rates were consistent with reference measurements performed with a pH electrode. The time response of Em_r and Ex_r method enabled measurement every 0.8 s and 4.5 s, respectively. The quantifiable rates lay in the range 0.004 - 0.1 pH-units s^{-1} (Figure S3). Ex_r and Em_r offered adequate resolution in the pH range 6.00 - 8.00 and 6.60 - 8.40, respectively, each with an uncertainty of approximately 0.05 (Figure S3). Importantly, sYFP showed no signs of degradation when tested for photostability (Figure S4).

3.2. Immobilization of sYFP to generate internally pH-sensitive materials

To apply sYFP for pH sensing within solid porous matrix, it is necessary to prepare a bioconjugate material suitably functionalized with sYFP on the internal pore surface. Procedure applicable to a representative variety of materials for efficient and controllable immobilization of sYFP was established in here. Besides stable binding to the solid surface, elements considered vital for sYFP immobilization were retention of the native pH response and uniform distribution of immobilized protein within solid matrix. Affinity-based oriented immobilization of sYFP, via the strong binding of an oligo-histidine peptide genetically fused to the protein's N-terminus with chelated metal ions (e.g. Ni^{2+}) on the surface of the solid material, was used to these ends. Note

that surface modification with metal-chelating groups is commonly used across materials, organic and inorganic.

Proof of concept for pH sensing with immobilized sYFP was obtained using cross-linked agarose particles, activated for immobilization via chelated Ni^{2+} groups (Ag-Ni). To ensure that sYFP did not immobilize only in the outer areas of Ag-Ni particles (Figure 1), it was essential to slow down the protein's immobilization rate by a competing ligand, which here was imidazole. By applying a gradually decreasing concentration of imidazole, a fairly uniform distribution of the immobilized sYFP was obtained at 1% (by weight) protein loading, as shown in Figure 1 and Figure S5. It is practically significant, for it simplifies experimental procedures greatly, that sYFP could be immobilized directly, i.e., without prior purification, from the complex matrix of proteins comprised in bacterial cell extract (Figure S5). As shown in Figure 1, the pH response of the Ag-Ni immobilizate of sYFP was identical within error limit (±2%) to that of the soluble protein. Apparent p*K*' values determined from pH dependencies of the ratiometric signal *R* were 7.01 and 7.73 for Ex_r and Em_r, respectively. These p*K*'s were similar for immobilized compared to soluble sYFP, implying a largely unperturbed pH sensor function of the sYFP bound to Ag-Ni.

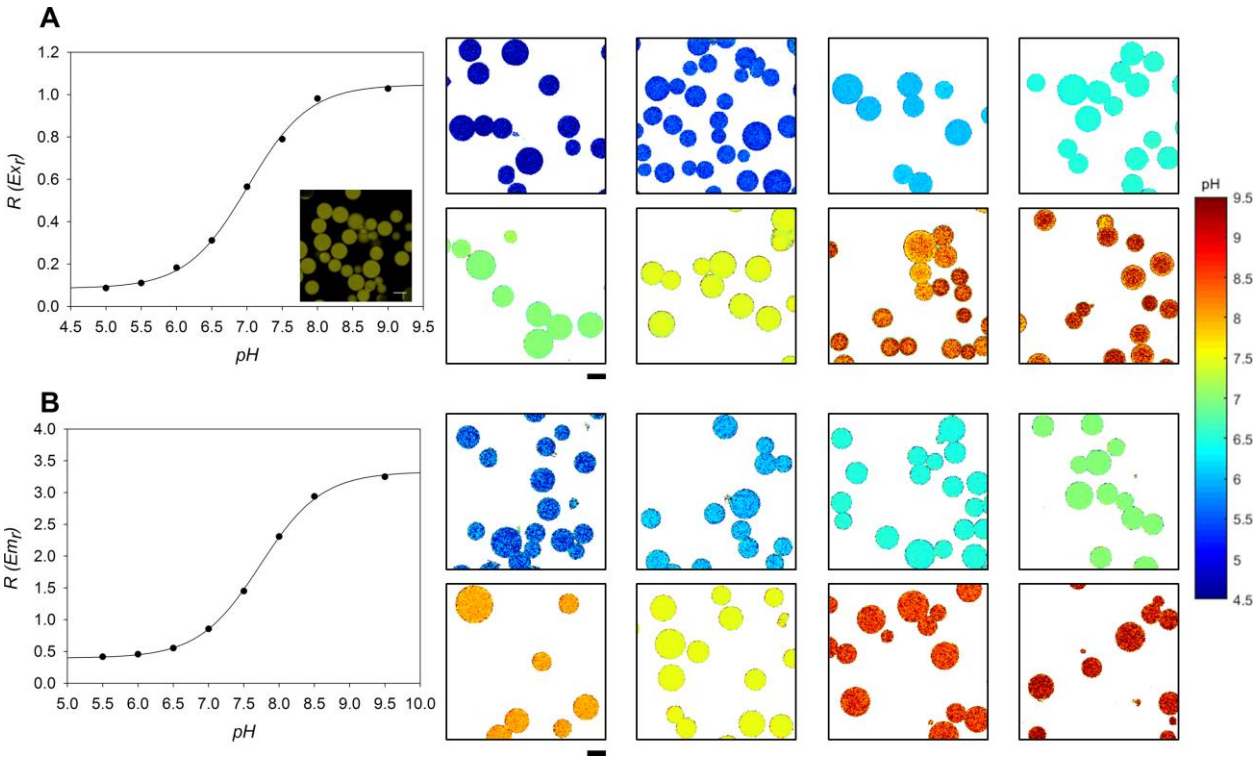

Figure 1. The pH response of sYFP immobilized in Ag-Ni is shown using (A) Ex_r and (B) Em_r. *R* (Ex_r) is the ratiometric signal for Ex_r defined as: F(488, 500-600)/F(458, 500-600). *R* (Em_r) is the ratiometric signal for Em_r defined as: F(458, 515-600)/F(458, 475-515). Each point in the graph represents the space-averaged mean of five ROIs analyzed. The plots of *R* dependent on pH were obtained using Equation. 1. The inset in panel (A) is a confocal image showing the homogeneous distribution of sYFP in Ag-Ni. The scale bar is 100 micrometer.

Using the same proton-releasing enzymatic reaction in solution as described above, dynamic response of the pH-sensitive material was analyzed, as shown in Figure 2. Rates of pH decrease in the range 0.004 - 0.1 pH-units s^{-1} were accurately quantified. Using a threshold of ≤ 0.05 for the measurement error, Ex_r offered a suitable resolution in the pH range 5.50 - 8.10 whereas for Em_r this pH range was 6.00 - 8.50 (Figure S6). As with soluble sYFP, the immobilizate enabled data collection faster when Em_r was used while the dynamic range of pH measurement was larger

using Ex_r. We therefore conclude that sYFP immobilized to Ag-Ni constituted a functional and practically useful opto-chemical sensor material for ratiometric pH measurement.

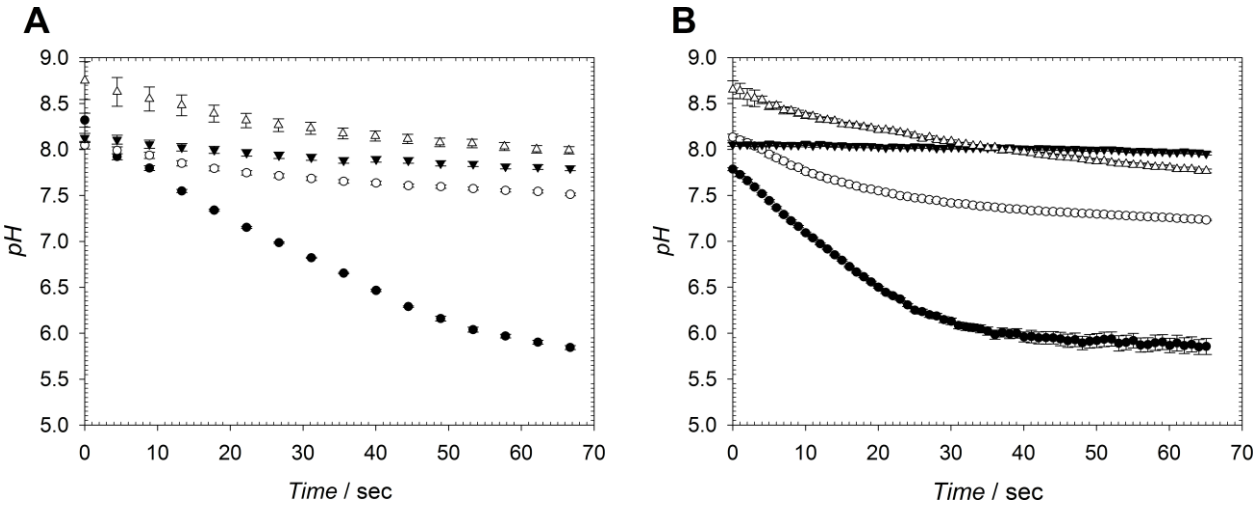

Figure 2. The dynamic response of sYFP immobilized onto Ag-Ni is shown. Each panel shows the space-averaged pH time courses during the hydrolysis of 10 mM PenG catalyzed by soluble PGA. Time courses were measured with (A) Ex_r and (B) Em_r at 10 mM sodium phosphate buffer using 30 U_{PenG} mL^{-1} (●), 3 U_{PenG} mL^{-1} (○) and 0.3 U_{PenG} mL^{-1} (▼) or in 100 mM sodium phosphate buffer using 30 U_{PenG} mL^{-1} (△). Uncertainties in the pH values determined were calculated according to Equation S6 and are shown with error bars. Every time course point corresponds to space-averaged pH within one ROI (one Ag-Ni particle), each time course is exemplary shown for multiple experiments performed.

3.3. Extending the immobilization of sYFP to other materials

Besides agarose, silica (glass) and methacrylate polymers have similarly widespread uses in biological studies, including enzyme immobilization, protein chromatography and adherent cell growth.[51–53] Unlike agarose, which stands for a class of materials derived from natural macromolecules, silica (glass) and methacrylate polymers represent materials of completely different nature. To expand the concept of internal pH sensing also to these materials, sYFP was immobilized on controlled pore glass (CPG-Ni) and polymethacrylate porous particles (Sep-Ni), each having chelated Ni^{2+} groups on their surface. As shown in Figure 3, sYFP immobilized at

1% (by weight) protein/carrier loading appeared to have become uniformly distributed in both materials. Irrespective of Ex_r and Em_r used, both materials gave suitable signal-to-noise ratios (2 %). Their respective *R* signals exhibited sigmoidal pH-dependence (Figure 3, Figure S6 - S9) from which the apparent p*K*' and the dynamic range of measurement were determined (Table 1). A slight downshift in the p*K*'s for the CPG-Ni by about 0.2 pH units compared to other immobilizates of sYFP might be a consequence of the relatively higher surface acidity of the CPG material.

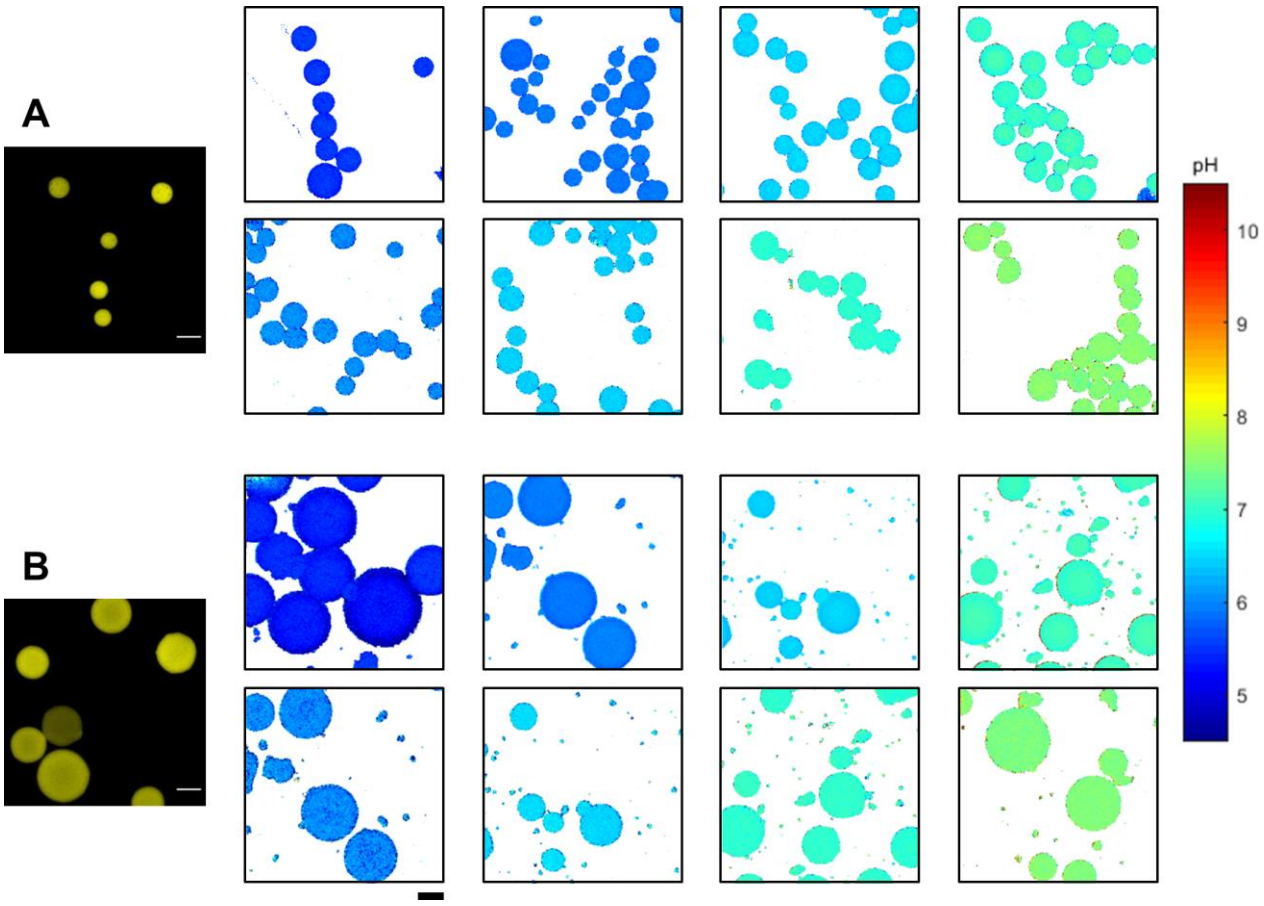

Figure 3. The pH response of sYFP immobilized onto (A) CPG-Ni and (B) Sep-Ni is shown. Each panel shows an intensity image of the fluorescent material and the pH images at different values within the dynamic range. The first row in each panel corresponds to Ex_r, the second to Em_r. The scale bar is 100 micrometer.

Common caveat against the immobilization by affinity to chelated metals is protein leakage, in consequence of a binding process that is fully reversible in principle. Therefore, despite sYFP's binding to each material was extremely stable, we sought to demonstrate that pH sensing with immobilized sYFP was not restricted to a single method of protein immobilization. To this end, covalent attachment of sYFP to agarose activated with glyoxyl groups was used. This is a common way of immobilizing proteins in a nondissociable form via multiple covalent linkages with the material surface. As for the immobilization by affinity, attention was required to ensure uniform distribution of the covalently immobilized sYFP in the solid matrix (Figure S10). Parameters characterizing the pH sensor function of sYFP immobilized on Ag-Gly are summarized in Table 1, Figure S7 and Figure S11. The covalent immobilizate of sYFP was usable for pH determination with characteristics only marginally different from those of the noncovalent immobilizates.

3.4 Spatiotemporally resolved pH mapping in solid materials

3.4.1 Heterogeneous biocatalytic reaction in pH-sensor porous material

Biochemical reactions involving consumption or production of proton are of immediate relevance to be studied with the pH-sensor materials developed. Especially, when these reactions take place confined inside a porous material, due to as immobilized enzyme for instance, differences between pH in solution and within the solid are expected. The spatiotemporal mapping of the internal pH becomes then vital to characterize, and so optimize, the overall system performance. Employing penicillin G acylase immobilized on agarose we sought to demonstrate the important advance made through sYFP. To show that the immobilization of sYFP and enzyme together on the same material was flexible (i.e., did not by necessity have to occur via the same

immobilization principle), we first immobilized the enzyme covalently[54] and attached sYFP later by binding it to chelated Ni^{2+}. Material heterofunctionalization (Ag-Ni-Gly) that enables protein colocalization via distinct surface chemistries, each suitable for the individual protein, was developed in earlier work.[55] The Supporting Information summarizes the results obtained for the coimmobilizate of enzyme and sYFP (Figure S12, Figure S13 and Table S1). Co-immobilization of the two proteins did not affect their individual properties. The pH response characteristics of sYFP immobilized alone and together with the acylase were identical. Hydrolysis of penicillin G by the immobilized acylase was unaffected by immobilized sYFP. Collectively, the contention of sYFP constituting a pH sensor of excellent biocompatibility is strongly supported by these findings.

3.4.2 Dynamics of internal pH due to immobilized enzymatic reaction

A reaction setup was used in which agarose particles containing immobilized sYFP and PGA (catalyst particle) were kept static in stagnant suspension. The experiment was designed to monitor the initial reaction rate, immediately after addition of the substrate. The measurement provides one data point per 0.8 s, enabling convenient resolution of the transient phase before the coupled reaction and diffusion reach steady state. Particles containing sYFP but lacking the enzyme (bulk particle) were used as external reference, to record the pH in solution. These bulk particles are distinguished from the particles containing sYFP and enzyme (catalyst particle) by their smaller size, as shown in Figure 4. An exemplary pH mapping of a reaction course based on the analysis of two bulk particles (ROI 1 and ROI 2) and two catalyst particles (ROI 3 and ROI 4) is shown in Figure 4A. The time course of space-averaged pH within the particles is shown in Figure 4B. The bulk particle (ROI 1) revealed a slow pH decrease corresponding to the expected

acidification rate in solution (~0.005 pH-units s^{-1}). The catalyst particles (ROI 3 and ROI 4), by contrast, showed steep internal acidification (Figure 4B). The time course consists of a pronounced pH drop within the first seconds of reaction followed by a slower phase of pH decrease. At apparent steady state, a pH difference of ~1.5 pH units between bulk (ROI 1) and the catalyst particles prevailed. Both dynamics and magnitude of the pH gradient reflect coupling of proton-releasing reaction confined to the solid surface of the catalyst particle's pores and the molecular diffusion events inside these pores. The pH gradient at steady state is determined by the ratio of characteristic times (the reciprocal first-order rate constants) of diffusion and reaction. Progress towards steady state is observed in the initial excursion of the internal pH. The characteristic time of reaction is inversely proportional to the enzyme activity immobilized, while the characteristic time of diffusion is mainly dependent on the pore size, form and particle radius. The pH drop inside the particle may affect the activity and stability of the immobilized enzyme, its stability or both. Measurement of internal pH therefore enables one to disentangle the complex interplay of factors in a solid immobilizate, thus gaining improved understanding as a basis for further design and optimization. It is emphasized here that a uniform pH decrease was observed in all the regions of interest (ROIs) analyzed when only bulk particles and equivalent volumetric activity of acylase were used. This result effectively eliminates the possibility of concentration gradients caused by a slow distribution of the substrate within the reaction medium, as is shown in Figure S14, Video S1and S2 in the Supporting Information.

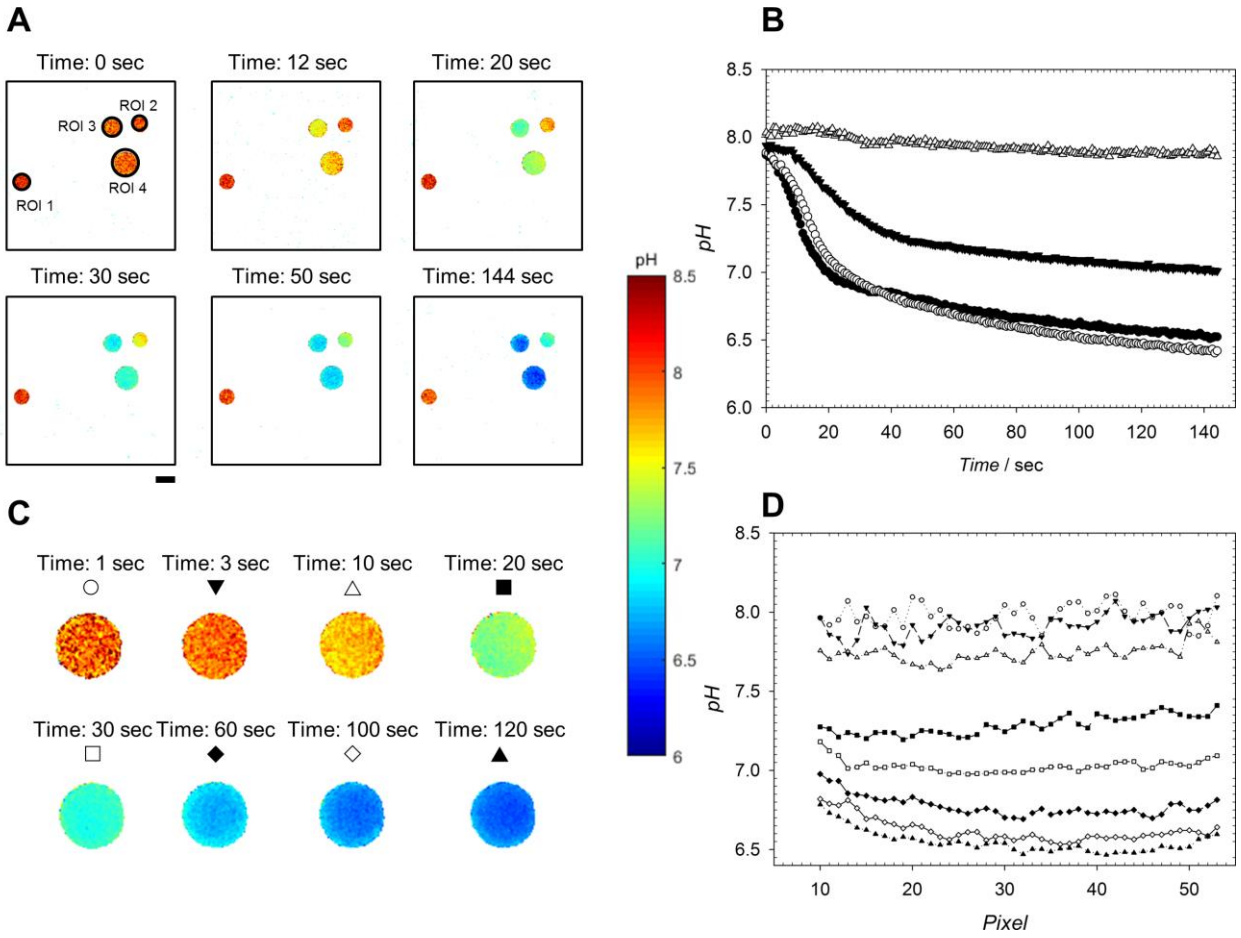

Figure 4. Spatiotemporal mapping of pH in the reactions catalyzed by a sYFP-PGA-coimmobilizate on Ag-Ni-Gly measured with Em_r.is shown. The PGA loading was 805 U_{PenG} g^{-1} and 20 mM PenG in 10 mM sodium phosphate buffer were used. (A) The pH maps of various sYFP-PGA-coimmobilizates and bulk particles at different time points are shown. ROIs used for analysis in (B) are highlighted with a black circle; ROI 1 and 2 are bulk particles, ROI 3 and 4 are catalyst particles. The scale bar is 100 μm. (B) Space averaged pH time courses of the 4 different ROIs highlighted in (A). ROI 1 (△) and ROI 2 (▼) ROI 3 (●) and ROI 4 (○). (C) Details of pH mapping in ROI 4 are shown. (D) The pH profiles across the center of the bead in ROI 4 at different times are shown. The data are obtained from the pH maps in panel C. One pixel corresponds to 2.3 micrometer.

Besides showing the internal pH drop in the catalyst particles, Figure 4 additionally reveals lowering of pH in the liquid immediately surrounding these particles, this can be observed by following the pH within bulk particles located at different distances of catalyst particle. In ROI 2,

for instance, the pH rapidly dropped to 7.5, and then decreased more slowly to a value of 7.2, while the pH in ROI 1 was almost constant at ~8 throughout. The finite diffusivity of protons released from the particles into the bulk solution is the cause of this locally lowered pH in the vicinity of the particles. The stronger decrease of pH in ROI 2 as compared to ROI 1 can be explained by smaller distance to the catalyst particles, ROI 3 as compared to ROI 4. It is expected that agitation of the solution containing the particles, as in stirred reactors, would eliminate the local pH decrease around the particles by enhancing the dispersion of protons into the bulk solution in comparison with pure diffusion. However, the internal diffusion in pores would be unaffected by agitation. Figure S15 shows the results of a similar set of experiments in which Ex_r was recorded. The evidences obtained from measurements of Em_r and Ex_r were fully consistent with each other. Full videos of time-resolved microscopic imaging analysis are shown in the Supporting Information.

We show that this experimental setup enables spatially resolved pH measurements within individual particles simultaneously, covering a spatial range from µm to almost mm. A magnification of catalyst particle ROI 4 is shown in Figure 4C and the spatial profile is depicted in Figure 4D. In the kinetic transient (≤ 30 s) involving fast drop of internal pH, a relatively flat pH profile was observed along the particle's radius. Therefore, this indicated that the initial diffusion of substrate into the catalyst particle was sufficient to support a spatially uniform internal acidification rate. In contrast, the internal pH profile in steady state was bent upward slightly at the sides. This suggested that the overall acidification rate in the center of the catalyst particle was substantially higher than in the outer regions, likely a result of "buffering" effect from the external bulk. Thus, spatiotemporally resolved pH mapping in porous matrices represents an advanced tool for the characterization of solid-enzyme immobilizates with real-time

tracking of the reaction microenvironment. This can be applied to any reaction involving proton release or uptake. Not only can it be used in the analysis of enzymatic initial rates examined with microscopic imaging as shown, but it can also be adapted to essentially all devices for practical application of immobilized enzymes when given suitable modifications (e.g. fixed-bed reactor operated under continuous fluid flow).

3.4.3 Factors influencing the internal pH change in solid enzyme immobilizate

As mentioned previously, the internal pH drop in penicillin G acylase immobilizates relative to the pH in bulk solution reflects the interplay between biocatalytic reaction and diffusion within porous solids.[29,31,32,56,57] Since the reaction rate scales directly with the amount of enzyme activity immobilized, one expects the internal pH to decrease in response to increased loading of enzyme activity. Magnitude of the pH drop may be limited physically by the rate of pore diffusion or biologically by the effect of low pH on the enzyme's activity or stability. Figure 5A (Em_r) and Figure S16 (Ex_r) show time courses of the internal pH gradient (ΔpH = space-averaged pH in solid - pH in bulk) for enzyme immobilizates differing in the penicillin G acylase activity loaded (between 27 and 805 U_{PenG} g^{-1}). While at low enzyme loading the internal pH was hardly different from the pH in bulk after substrate addition, increased enzyme loadings gave rise to a substantial ΔpH at steady state of up to –1.6 pH units (Figure 5A). Note: this ΔpH is sufficient to result in a significant change in the behavior of most enzymes. As with previous experiments, the time courses displayed a rapid initial drop in pH for roughly 30 s and a much slower decrease in pH afterwards, indicating that the progressing acidification of the bulk solution was due to the enzymatic conversion. Control reactions conducted with free penicillin G acylase showed that the

distribution of substrate in the stagnant suspension of particles was fast compared to the enzymatic conversion. It so did not affect the measurements performed.

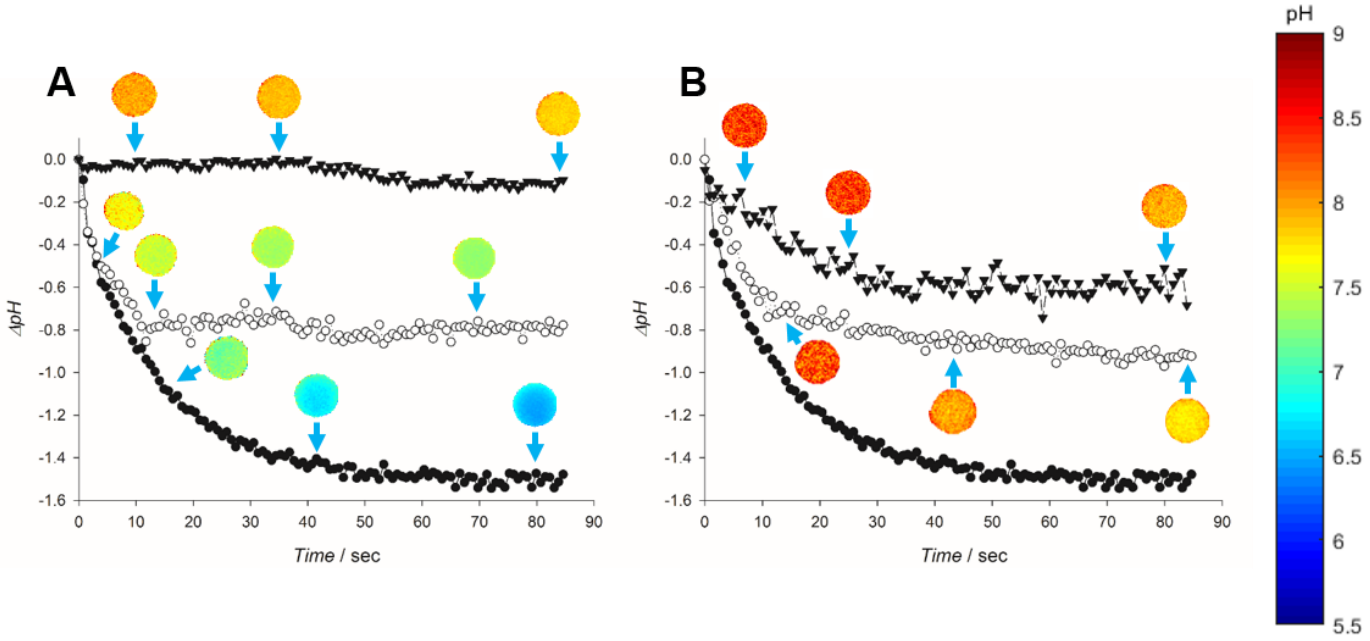

Figure 5. The evolution of ΔpH (internal pH - bulk pH) in reaction time courses of YFP-PGA-coimmobilizates on Ag-Ni-Gly measured with Em_r is shown. Panel (A) shows the effect of the enzyme loadings: 805 U_{PenG} g^{-1} (●), 130 U_{PenG} g^{-1} (○) and 27 U_{PenG} g^{-1} (▼). Panel (B) shows the effect of the sodium phosphate buffer concentration: 10 mM (●), 100 mM (○) and 200 mM (▼). The PGA loading was 805 U_{PenG} g^{-1} of carrier and 20 mM PenG were used. Images of catalyst particles corresponding to each reaction are shown for different time points (blue arrows).

We next tested the effects of buffer concentration on ΔpH. To that end, we measured ΔpH of penicillin hydrolysis in sodium phosphate buffer of concentration ranging from 10 mM to 200 mM. To achieve a rapid and large drop in the pH (see Figure 5A), a high enzyme loading of 805 U_{PenG} g^{-1} of carrier was used. Time courses of ΔpH for the three buffer conditions are summarized in Figure 5B. We found that increased concentration of sodium phosphate potently slowed down the pH drop, but also reduced the magnitude of pH change at steady state. However, the internal

pH drop was still present even in the 300 mM buffer (ΔpH = –0.6). Therefore, this clearly showed that it was important to record the internal ΔpH under all conditions tested.

4. CONCLUSION

The current study reveals sYFP as a powerful pH indicator for ratiometric optical sensing applications in real time within porous materials. A number of properties make sYFP specifically suited for pH sensing in biological systems. First, the dynamic range of its pH response (6.0 to 8.4) covers well the pH ranges in which most biological systems function optimally and are therefore used in practice. Second, due to its highly stable nature, sYFP is compatible with many different proteins (e.g., enzymes) and adapts well to the conditions required for these proteins. Functional incorporation of sYFP into a representative selection of porous materials is demonstrated here via an immobilization that involves controllable orientation of the protein attached to the solid surface. Moreover, the industrially-relevant example of penicillin G acylase hydrolyzing penicillin G with concomitant release of proton is used to show application of the sYFP-based pH sensing method for spatiotemporally resolved mapping of pH gradients in solid enzyme immobilizates containing the sYFP co-immobilized. This method provides, for the microscopy settings used, a time resolution (time to provide a data point) of 0.8s for Em_r and 4.5s for Ex_r, this is typically sufficient to evaluate enzymatic reactions, as shown in the experiments, and many other biological processes in general, at steady state.. Importance of the method for advanced (real-time) characterization of solid porous biocatalysts, and so their design and optimization, is demonstrated. Application to a broad variety of materials, and biology incorporated by them, seems possible. Optical pH sensing in solid materials based on sYFP is applicable to microscopic imaging analysis, as shown here. However, the technique can be

readily adapted to various formats of analytical read-out, such as microplate readers, optical fibers and reaction set-ups (e.g. flow systems). Possible uses involve high-through screening and real-time monitoring of pH changes in solid materials during bioprocessing. Finally, the sYFP system represents a novel pH-sensing platform that could find application widely across the biosciences.

ASSOCIATED CONTENT

Supporting Information. Preparation of the materials used, the assays applied, the pH calculation, error propagation analysis and principal component analysis are shown (Supporting methods). Spectra of soluble sYFP (Figure S1); dependence of fluorescence ratio *R* for soluble sYFP on pH (Figure S2); pH time courses for the hydrolysis of PenG catalyzed by soluble PGA (Figure S3); photobleaching analysis of soluble sYFP (Figure S4); immobilization of sYFP on Ag-Ni (Figure S5); uncertainty in the calculation of the measured pH at different pH values for the different materials used (Figure S6); pH response curves obtained for sYFP immobilized on different materials (Figure S7); analysis of dynamic pH response of sYFP-CPG-Ni (Figure S8); analysis of the dynamic response of sYFP-Sep-Ni (Figure S9); pH response of sYFP-Ag-Gly (Figure S10); analysis of the dynamic response of sYFP-Ag-Gly (Figure S11); characterization of PGA immobilized onto Ag-Ni-glyoxyl (Figure S12); dependence of fluorescence ratio onto pH for sYFP-PGA-Ag-Ni-Gly coimmobilizate (Figure S13); spatiotemporal mapping of pH by sYFP immobilized into Ag-Ni (Figure S14); spatiotemporal mapping of pH catalyzed by a sYFP-PGA-coimmobilizate on Ag-Ni-Gly measured with Ex_r (Figure S15); ΔpH time courses catalyzed by a sYFP-PGA-coimmobilizate on Ag-Ni-Gly measured with Ex_r (Figure S16); characterization of a sYFP-PGA-coimmobilizate as ratiometric pH sensors (Table S1); two videos showing time-

resolved imaging of pH in particles of conditions analyzed in Figure S14 (Video S1 and Video S2).

AUTHOR INFORMATION

Corresponding Author

Prof. Bernd Nidetzky, Institute of Biotechnology and Biochemical Engineering, Graz University of Technology, NAWI Graz, Petersgasse 12, A-8010 Graz, Austria; phone: +43 316 873 8400; fax: +43 316 873 8434; e-mail: bernd.nidetzky@tugraz.at

Author Contributions

The manuscript was written through contributions of all authors. All authors have given approval to the final version of the manuscript. TC, JMB and BN designed the research. TC performed experiments. TC and JMB analyzed data. AH and JB prepared the sYFP. TC, JMB and JMG designed the protein immobilization. ZP analyzed spectral properties and pH response of sYFP. TC, JMB and BN wrote the paper.

ACKNOWLEDGEMENTS

JMG acknowledges the Spanish Government for financial support (CTQ2015-70348-C2-1-R). JB and AH acknowledge funding from the Spanish Ministry of Economy and Competitiveness through grant BIO2013-44963R and from the Ramón Areces Foundation to CBMSO.

REFERENCES

(1) Banani, S. F.; Lee, H. O.; Hyman, A. A.; Rosen, M. K. Biomolecular Condensates: Organizers of Cellular Biochemistry. *Nat. Rev. Mol. Cell Biol.* **2017**, *18*, 285–298.

(2) Ellis, R. J. Macromolecular Crowding: An Important but Neglected Aspect of the Intracellular Environment. *Curr. Opin. Struct. Biol.* **2001**, *11*, 114–119.

(3) Kuznetsova, I. M.; Turoverov, K. K.; Uversky, V. N. What Macromolecular Crowding Can Do to a Protein. *Int. J. Mol. Sci.* **2014**, *15*, 23090–23140.

(4) Ellis, R. J.; Minton, A. P. Cell Biology: Join the Crowd. *Nature* **2003**, *425*, 27–28.

(5) Rivas, G.; Minton, A. P. Macromolecular Crowding In Vitro, In Vivo, and In Between. *Trends Biochem. Sci.* **2016**, *41*, 970–981.

(6) Ross, J. L. The Dark Matter of Biology. *Biophys. J.* **2016**, *111*, 909–916.

(7) Pronk, S.; Lindahl, E.; Kasson, P. M. Dynamic Heterogeneity Controls Diffusion and Viscosity near Biological Interfaces. *Nat. Commun.* **2014**, *5*, 3034.

(8) Ando, T.; Skolnick, J. Crowding and Hydrodynamic Interactions Likely Dominate in Vivo Macromolecular Motion. *Proc. Natl. Acad. Sci.* **2010**, *107*, 18457–18462.

(9) Avnir, D.; Coradin, T.; Lev, O.; Livage, J. Recent Bio-Applications of Sol–gel Materials. *J Mater Chem* **2006**, *16*, 1013–1030.

(10) York-Duran, M. J.; Godoy-Gallardo, M.; Labay, C.; Urquhart, A. J.; Andresen, T. L.; Hosta-Rigau, L. Recent Advances in Compartmentalized Synthetic Architectures as Drug Carriers, Cell Mimics and Artificial Organelles. *Colloids Surf. B Biointerfaces* **2017**, *152*, 199–213.

(11) Han, F.; Qi, X.; Li, L.; Bu, L.; Fu, Y.; Xie, Q.; Guo, M.; Li, Y.; Ying, Y.; Yao, S. Bio-Inspired Preparation of Fibrin-Boned Bionanocomposites of Biomacromolecules and Nanomaterials for Biosensing. *Adv. Funct. Mater*. **2014**, *24*, 5011–5018.

(12) Wronska, M. A.; O'Connor, I. B.; Tilbury, M. A.; Srivastava, A.; Wall, J. G. Adding Functions to Biomaterial Surfaces through Protein Incorporation. *Adv. Mater.* **2016**, *28* (27), 5485–5508.

(13) Owens, G. J.; Singh, R. K.; Foroutan, F.; Alqaysi, M.; Han, C.-M.; Mahapatra, C.; Kim, H.-W.; Knowles, J. C. Sol–gel Based Materials for Biomedical Applications. *Prog. Mater. Sci.* **2016**, *77*, 1–79.

(14) Ruiz-Hitzky, E.; Darder, M.; Aranda, P.; Ariga, K. Advances in Biomimetic and Nanostructured Biohybrid Materials. *Adv. Mater.* **2010**, *22*, 323–336.

(15) Blanchette, C. D.; Knipe, J. M.; Stolaroff, J. K.; DeOtte, J. R.; Oakdale, J. S.; Maiti, A.; Lenhardt, J. M.; Sirajuddin, S.; Rosenzweig, A. C.; Baker, S. E. Printable Enzyme-Embedded Materials for Methane to Methanol Conversion. *Nat. Commun.* **2016**, *7*, 11900.

(16) Küchler, A.; Yoshimoto, M.; Luginbühl, S.; Mavelli, F.; Walde, P. Enzymatic Reactions in Confined Environments. *Nat. Nanotechnol.* **2016**, *11*, 409–420.

(17) Sanchez, C.; Belleville, P.; Popall, M.; Nicole, L. Applications of Advanced Hybrid Organic–inorganic Nanomaterials: From Laboratory to Market. *Chem. Soc. Rev.* **2011**, *40*, 696–753.

(18) Torres-Salas, P.; del Monte-Martinez, A.; Cutiño-Avila, B.; Rodriguez-Colinas, B.; Alcalde, M.; Ballesteros, A. O.; Plou, F. J. Immobilized Biocatalysts: Novel Approaches and Tools for Binding Enzymes to Supports. *Adv. Mater.* **2011**, *23*, 5275–5282.

(19) Bae, J.-S.; Jeon, E.; Moon, S.-Y.; Oh, W.; Han, S.-Y.; Lee, J. H.; Yang, S. Y.; Kim, D.-M.; Park, J.-W. Bicontinuous Nanoporous Frameworks: Caged Longevity for Enzymes. *Angew. Chem. Int. Ed.* **2016**, *55*, 11495–11498.

(20) Bolivar, J. M.; Consolati, T.; Mayr, T.; Nidetzky, B. Shine a Light on Immobilized Enzymes: Real-Time Sensing in Solid Supported Biocatalysts. *Trends Biotechnol.* **2013**, *31*, 194–203.

(21) Bolivar, J. M.; Eisl, I.; Nidetzky, B. Advanced Characterization of Immobilized Enzymes as Heterogeneous Biocatalysts. *Catal. Today* **2016**, *259*, 66–80.

(22) Carlsson, N.; Gustafsson, H.; Thörn, C.; Olsson, L.; Holmberg, K.; Åkerman, B. Enzymes Immobilized in Mesoporous Silica: A Physical-Chemical Perspective. *Adv. Colloid Interface Sci.* **2014**, *205*, 339–360.

(23) Casey, J. R.; Grinstein, S.; Orlowski, J. Sensors and Regulators of Intracellular PH. *Nat. Rev. Mol. Cell Biol.* **2010**, *11*, 50–61.

(24) Yang, Z.; Cao, J.; He, Y.; Yang, J. H.; Kim, T.; Peng, X.; Kim, J. S. Macro-/Micro-Environment-Sensitive Chemosensing and Biological Imaging. *Chem. Soc. Rev.* **2014**, *43*, 4563–4601.

(25) Yamaguchi, A.; Namekawa, M.; Kamijo, T.; Itoh, T.; Teramae, N. Acid−Base Equilibria inside Amine-Functionalized Mesoporous Silica. *Anal. Chem.* **2011**, *83*, 2939–2946.

(26) Sun, X.; Xie, J.; Xu, J.; Higgins, D. A.; Hohn, K. L. Single-Molecule Studies of Acidity Distributions in Mesoporous Aluminosilicate Thin Films. *Langmuir* **2015**, *31*, 5667–5675.

(27) Begemann, J.; Spiess, A. C. Dual Lifetime Referencing Enables PH-Control for Oxidoreductions in Hydrogel-Stabilized Biphasic Reaction Systems. *Biotechnol. J.* **2015**, *10*, 1822–1829.

(28) Huang, H. Y.; Shaw, J.; Yip, C.; Wu, X. Y. Microdomain PH Gradient and Kinetics inside Composite Polymeric Membranes of PH and Glucose Sensitivity. *Pharm. Res.* **2008**, *25*, 1150–1157.

(29) Boniello, C.; Mayr, T.; Klimant, I.; Koenig, B.; Riethorst, W.; Nidetzky, B. Intraparticle Concentration Gradients for Substrate and Acidic Product in Immobilized Cephalosporin C Amidase and Their Dependencies on Carrier Characteristics and Reaction Parameters. *Biotechnol. Bioeng.* **2010**, *106*, 528–540.

(30) Zahel, Thomas; Boniello, Caterina; Nidetzky, Bernd. Real-Time Measurement and Modeling of Intraparticle pH Gradient Formation in Immobilized Cephalosporin C Amidase. *Proccess Biochem.* **2013**, *48*, 593–604.

(31) Spiess, A.; Schlothauer, R.; Hinrichs, J.; Scheidat, B.; Kasche, V. PH Gradients in Immobilized Amidases and Their Influence on Rates and Yields of Beta-Lactam Hydrolysis. *Biotechnol. Bioeng.* **1999**, *62*, 267–277.

(32) Spiess, A. C.; Kasche, V. Direct Measurement of PH Profiles in Immobilized Enzyme Carriers during Kinetically Controlled Synthesis Using CLSM. *Biotechnol. Prog.* **2001**, *17*, 294–303.

(33) Wencel, D.; Abel, T.; McDonagh, C. Optical Chemical PH Sensors. *Anal. Chem.* **2014**, *86*, 15–29.

(34) Barczak, M.; McDonagh, C.; Wencel, D. Micro- and Nanostructured Sol-Gel-Based Materials for Optical Chemical Sensing (2005–2015). *Microchim. Acta* **2016**, *183*, 2085–2109.

(35) Luo, H.; Zhu, L.; Chang, Y.; Liu, X.; Liu, Z.; Sun, H.; Li, X.; Yu, H.; Shen, Z. Microenvironmental PH Changes in Immobilized Cephalosporin C Acylase during a

Proton-Producing Reaction and Regulation by a Two-Stage Catalytic Process. *Bioresour. Technol.* **2017**, *223*, 157–165.

(36) Boniello, C.; Mayr, T.; Bolivar, J. M.; Nidetzky, B. Dual-Lifetime Referencing (DLR): A Powerful Method for on-Line Measurement of Internal PH in Carrier-Bound Immobilized Biocatalysts. *BMC Biotechnol.* **2012**, *12*, 11.

(37) Day, R. N.; Davidson, M. W. The Fluorescent Protein Palette: Tools for Cellular Imaging. *Chem. Soc. Rev.* **2009**, *38*, 2887–2921.

(38) Frommer, W. B.; Davidson, M. W.; Campbell, R. E. Genetically Encoded Biosensors Based on Engineered Fluorescent Proteins. *Chem. Soc. Rev.* **2009**, *38*, 2833–2841.

(39) Lippincott-Schwartz, J.; Patterson, G. H. Development and Use of Fluorescent Protein Markers in Living Cells. *Science* **2003**, *300*, 87–91.

(40) Dedecker, P.; De Schryver, F. C.; Hofkens, J. Fluorescent Proteins: Shine on, You Crazy Diamond. *J. Am. Chem. Soc.* **2013**, *135*, 2387–2402.

(41) Veselov, A. A.; Abraham, B. G.; Lemmetyinen, H.; Karp, M. T.; Tkachenko, N. V. Photochemical Properties and Sensor Applications of Modified Yellow Fluorescent Protein (YFP) Covalently Attached to the Surfaces of Etched Optical Fibers (EOFs). *Anal. Bioanal. Chem.* **2012**, *402*, 1149–1158.

(42) Makyła, K.; Müller, C.; Lörcher, S.; Winkler, T.; Nussbaumer, M. G.; Eder, M.; Bruns, N. Fluorescent Protein Senses and Reports Mechanical Damage in Glass-Fiber-Reinforced Polymer Composites. *Adv. Mater.* **2013**, *25*, 2701–2706.

(43) Mahon, M. J. PHluorin2: An Enhanced, Ratiometric, PH-Sensitive Green Florescent Protein. *Adv. Biosci. Biotechnol.* **2011**, *2*, 132–137.

(44) Bizzarri, R.; Arcangeli, C.; Arosio, D.; Ricci, F.; Faraci, P.; Cardarelli, F.; Beltram, F. Development of a Novel GFP-Based Ratiometric Excitation and Emission PH Indicator for Intracellular Studies. *Biophys. J.* **2006**, *90*, 3300–3314.

(45) Bizzarri, R.; Serresi, M.; Luin, S.; Beltram, F. Green Fluorescent Protein Based PH Indicators for in Vivo Use: A Review. *Anal. Bioanal. Chem.* **2009**, *393*, 1107–1122.

(46) Pédelacq, J.-D.; Cabantous, S.; Tran, T.; Terwilliger, T. C.; Waldo, G. S. Engineering and Characterization of a Superfolder Green Fluorescent Protein. *Nat. Biotechnol.* **2006**, *24*, 79–88.

(47) Aliye, N.; Fabbretti, A.; Lupidi, G.; Tsekoa, T.; Spurio, R. Engineering Color Variants of Green Fluorescent Protein (GFP) for Thermostability, PH-Sensitivity, and Improved Folding Kinetics. *Appl. Microbiol. Biotechnol.* **2015**, *99*, 1205–1216.

(48) Mateo, C.; Grazu, V.; Guisan, J. M. Immobilization of Enzymes on Monofunctional and Heterofunctional Epoxy-Activated Supports. In *Immobilization of Enzymes and Cells*; Guisan, J. M., Ed.; Humana Press: Totowa, NJ, 2013; Vol. 1051, pp 43–57.

(49) López-Gallego, F.; Fernandez-Lorente, G.; Rocha-Martin, J.; Bolivar, J. M.; Mateo, C.; Guisan, J. M. Stabilization of Enzymes by Multipoint Covalent Immobilization on Supports Activated with Glyoxyl Groups. In *Immobilization of Enzymes and Cells*; Guisan, J. M., Ed.; Humana Press: Totowa, NJ, 2013; Vol. 1051, pp 59–71.

(50) Bernal, C.; Sierra, L.; Mesa, M. Improvement of Thermal Stability of β-Galactosidase from Bacillus Circulans by Multipoint Covalent Immobilization in Hierarchical Macro-Mesoporous Silica. *J. Mol. Catal. B Enzym.* **2012**, *84*, 166–172.

(51) Leonard, M. New Packing Materials for Protein Chromatography. *J. Chromatogr. B. Biomed. Sci. App.* **1997**, *699*, 3–27.

(52) Cao, L. *Carrier-Bound Immobilized Enzymes: Principles, Application and Design*; Wiley-VCH Verlag GmbH & Co. KGaA: Weinheim, FRG, 2005.

(53) Cantone, S.; Ferrario, V.; Corici, L.; Ebert, C.; Fattor, D.; Spizzo, P.; Gardossi, L. Efficient Immobilisation of Industrial Biocatalysts: Criteria and Constraints for the Selection of Organic Polymeric Carriers and Immobilisation Methods. *Chem. Soc. Rev.* **2013**, *42*, 6262–6276.

(54) Alvaro, G.; Fernandez-Lafuente, R.; Blanco, R. M.; Guisán, J. M. Immobilization-Stabilization of Penicillin G Acylase from Escherichia Coli. *Appl. Biochem. Biotechnol.* **1990**, *26*, 181–195.

(55) Batalla, P.; Bolívar, J. M.; Lopez-Gallego, F.; Guisan, J. M. Oriented Covalent Immobilization of Antibodies onto Heterofunctional Agarose Supports: A Highly Efficient Immuno-Affinity Chromatography Platform. *J. Chromatogr. A* **2012**, *1262*, 56–63.

(56) Tischer, W.; Kasche, V. Immobilized Enzymes: Crystals or Carriers? *Trends Biotechnol.* **1999**, *17*, 326–335.

(57) Zahel, T.; Boniello, C.; Nidetzky, B. Real-Time Measurement and Modeling of Intraparticle PH Gradient Formation in Immobilized Cephalosporin C Amidase. *Process Biochem.* **2013**, *48*, 593–604.

Table of Contents

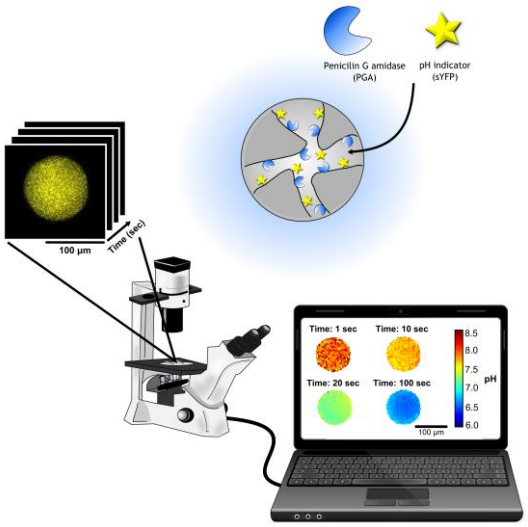

Supporting Information

Bio-based, internally pH sensitive materials: immobilized yellow fluorescent protein as optical sensor for spatiotemporal mapping of pH inside porous matrices

*Tanja Consolati[1], Juan M. Bolivar[1], Zdenek Petrasek[1], Aurelio Hidalgo[2], Jose Berenguer[2], Jose M. Guisán[3] and Bernd Nidetzky[1,4]**

[1] Institute of Biotechnology and Biochemical Engineering, Graz University of Technology, NAWI Graz, Petersgasse 12, A-8010 Graz, Austria

[2] Department of Molecular Biology, Universidad Autónoma de Madrid, Center for Molecular Biology 'Severo-Ochoa' (UAM-CSIC), Nicolás Cabrera 1, Madrid, Spain

[3] Institute of Catalysis and Petroleum Chemistry (ICP-CSIC), C/ Marie Curie, 2. Cantoblanco 28049. Madrid. Spain

[4] Austrian Centre of Industrial Biotechnology, Petersgasse 14, A-8010 Graz, Austria

[*] Corresponding Author

Prof. Bernd Nidetzky, Institute of Biotechnology and Biochemical Engineering, Graz University of Technology, NAWI Graz, Petersgasse 12, A-8010 Graz, Austria; phone: +43 316 873 8400; fax: +43 316 873 8434; e-mail: bernd.nidetzky@tugraz.at

Supporting methods

Preparation of materials

Epoxy activated agarose and glyoxyl agarose (Ag-Gly) were prepared as described previously.[1] Epoxy activated CPG was prepared according to a modified protocol from literature.[2] Briefly, the support (1.0 g wet weight) was activated in 30 mL toluene containing 5% GPMES under reflux at 105°C for 3 h. Gentle stirring was used. The support was washed with acetone and distilled water. Metal chelate supports (Ag-Ni, CPG-Ni and Sep-Ni) were prepared according to a modified protocol from literature.[3] The corresponding epoxy support (0.1 g wet weight/mL buffer) was activated with 0.9 g iminodiaceticacid in sodium bicarbonate buffer (100 mM at pH 11) under gentle stirring at room temperature for 2 h (agarose) or overnight (CPG and Sepabeads). Residual epoxy groups were hydrolyzed to glyceryl groups,[1] and the support was then washed with distilled water and incubated in 10 mg mL^{-1} $NiSO_4$ in distilled water for 30 min. Residual metal was washed away. All supports were dried and stored at 4°C.

Assays

The protein concentration was measured with a Roti®-Quant assay (Roth) referenced against known concentrations of BSA. The activity of soluble and immobilized PGA was determined spectrophotometrically using NIPAB as a substrate. A reported procedure from literature[4] was used. Alternatively, hydrolysis of PenG was measured.[5] Titration of the phenylacetic acid

released upon PenG hydrolysis (10 mM) was conducted with an automatic titrator (DL 50 Mettler Toledo). A final volume of 25 mL sodium phosphate buffer (0.1 M) at pH 7.50 was used. The temperature was 25°C. NaOH (25 mM) was used for titration. One activity unit (U_{PenG} or U_{NiPAB}) is the amount of PGA that hydrolyzes 1 µmol of PenG or NiPAB per minute. Under the applied conditions the ratio of activity between the two assays is 1.8 (= U_{PenG}/U_{NiPAB}).

Calculation of pH and error propagation analysis

We assumed that the concentration ratio of the protonated and deprotonated forms of sYFP was determined solely by the protonation equilibrium: c(protonated)/c(deprotonated) = $10^{pK\text{-}pH}$. Accordingly, fluorescence signals F_1 and F_2 measured in the two spectral channels would depend on pH in the following way,

$$F_1(pH) = \frac{H_1 + L_1 10^{pK-pH}}{1 + 10^{pK-pH}} \qquad \text{S1}$$

$$F_2(pH) = \frac{H_2 + L_2 10^{pK-pH}}{1 + 10^{pK-pH}} \qquad \text{S2}$$

In Equations S1 and S2, L_1 (L_2) and H_1 (H_2) are the fluorescence intensities in the channel 1 (2) at low and high pH, respectively.

The ratio R of these two fluorescence signals then depends on pH as shown in Equation S3:

$$R = \frac{F_1}{F_2} = \frac{H_1 + L_1 10^{pK-pH}}{H_2 + L_2 10^{pK-pH}} = R_0 \frac{R_{f+} 10^{pK'-pH}}{1 + 10^{pK'-pH}} \qquad \text{S3}$$

Where:

$$R_0 = \frac{L_1}{L_2}\,, R_f = \frac{L_2 H_1}{L_1 H_2} \text{ and } pK' = pK + \log_{10}\frac{L_2}{H_2} \qquad \text{S4}$$

The equation S3 is identical with Equation 1 in the main text, and can be used to calculate the pH from the experimental value of *R* (Equation 2 in main text).

The error σ_{pH} (standard deviation) of the experimentally determined pH depends on the error σ_R of the ratio *R*, which in turn depends on the experimental errors σ_{F1} and σ_{F2} of the two fluorescence intensities F_1 and F_2, as shown in Equation S5:

$$\sigma_{pH} = \left|\frac{\partial pH}{\partial R}\right| \sigma_R = \left|\frac{\partial pH}{\partial R}\right| \sqrt{\left(\frac{\partial R}{\partial F_1}\right)^2 \sigma_{F1}^2 + \left(\frac{\partial R}{\partial F_2}\right)^2 \sigma_{F2}^2} \quad \text{S5}$$

Equation S5 leads to Equation 6:

$$\sigma_{pH} = \frac{1}{\ln 10}\left|\frac{1}{R-R_0} + \frac{1}{R_0 R_f - R}\right| \sqrt{\frac{1}{F_2^2}\sigma_{F1}^2 + \frac{F_1^2}{F_2^4}\sigma_{F2}^2} \qquad \text{S6}$$

The error σ_R of the ratio *R* is not constant but depends on pH, as expressed by the term under the square root in the above Equation S6. This implies that the region of the highest sensitivity is not necessarily at the point of the steepest dependence of *R* on pH, that is at pH = p*K*´, as one might assume. The actual range of the highest sensitivity may be shifted from this point to lower or higher pH values (see Figure S6).

Principal Component Analysis of the fluorescence spectra.

Principal Component Analysis[6] (PCA) of a set of spectra measured at a range of pH values was used to identify the number of distinct species in the sample. The spectra were assembled columnwise into a matrix A, and the eigenvectors and the eigenvalues of the matrix AA^T were

calculated (A^T is the matrix transpose of A). Two of the calculated eigenvalues had considerably larger values than the remaining eigenvalues. This means that two components (species) are sufficient to describe the experimental spectra at all pH values.

The spectra of these two species, s_p and s_d, can be expressed as a linear combination of the two eigenvectors v_1, v_2 corresponding to the two largest eigenvalues obtained from PCA: $(s_p, s_d) = (v_1, v_2)T$, where T is the 2x2 transformation matrix. The transformation matrix T was found by minimizing the difference between the spectra expressed via v_1 and v_2 and the spectra expressed via s_p and s_d under the constraint of protonation equilibrium between the protonated (spectrum s_p, concentration c_p) and the deprotonated (spectrum s_d, concentration c_d) species: $c_p/c_d = 10^{pK-pH}$. This procedure yielded also the value of pK. The calculations were performed in Matlab.

Supporting Figures

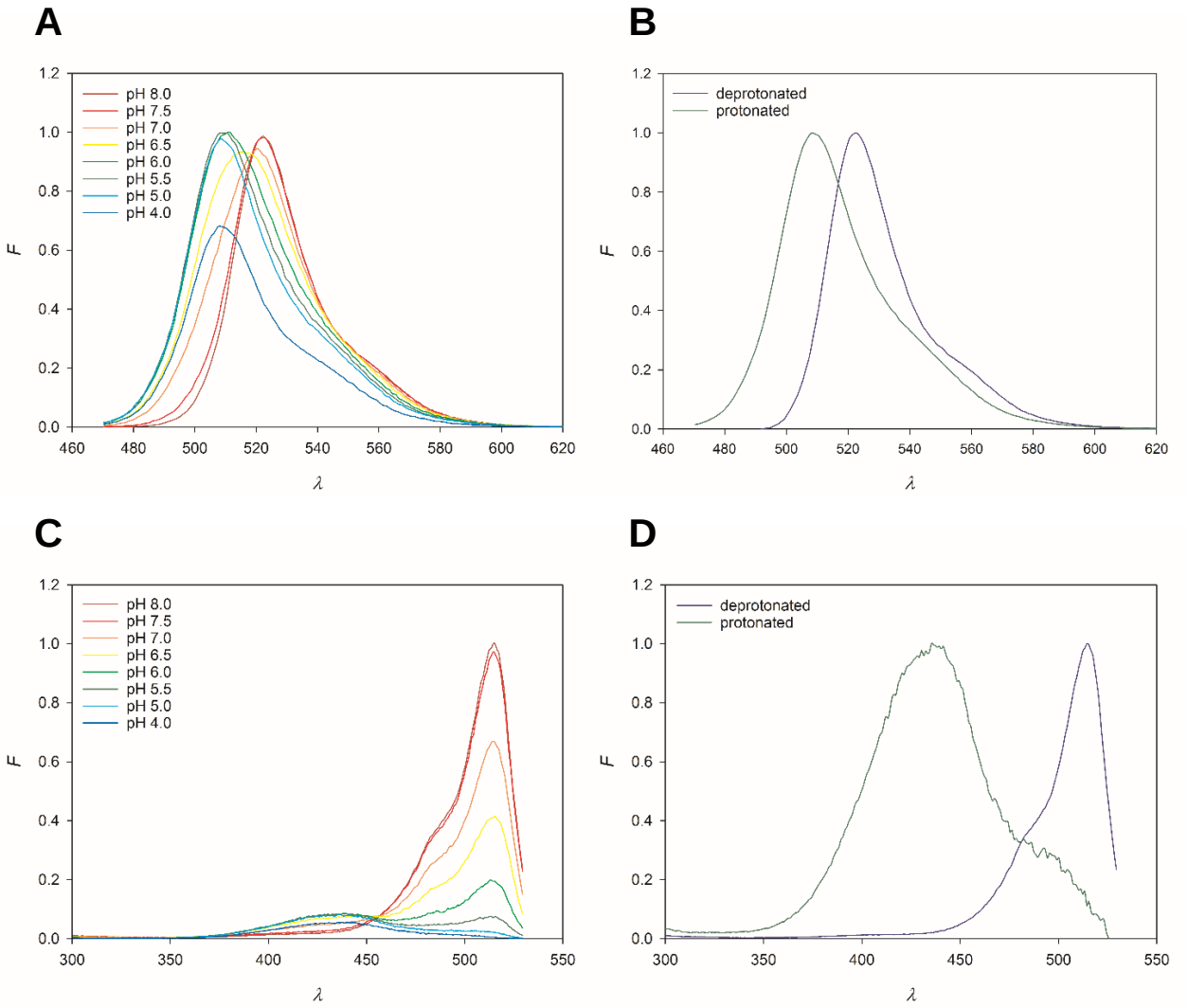

Figure S1. Emission (A) and excitation (C) spectra of sYFP measured at a range of pH values are shown together with results of principal component analysis (PCA) of the spectra (B, D). The excitation wavelength in A was 458 nm; the emission wavelength in C was 540 nm. Both the emission and the excitation spectra (A and C) exhibit an isosbestic point at a pH greater than 6, indicating the presence of two species (emission spectra: at 519 nm, excitation spectra: 456 nm). At lower pH values, the fluorescence is weaker, possibly indicating the emergence of another, multiply-protonated and weakly fluorescent or non-fluorescent species. (B) Emission spectra and

(D) excitation spectra of the protonated and deprotonated forms of sYFP were calculated from the corresponding spectra in A and B using PCA[6] with the assumption of a protonation equilibrium between the two species.

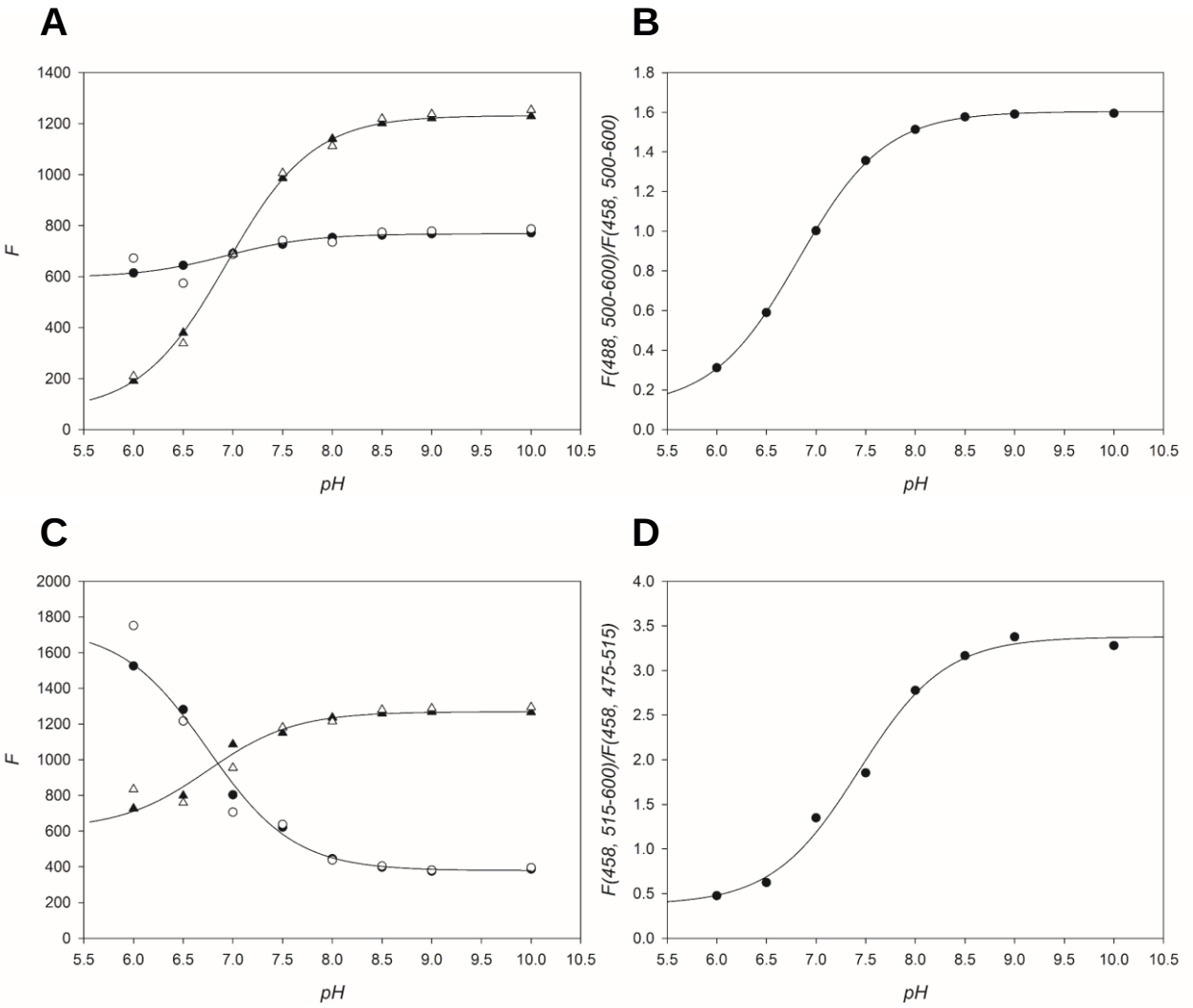

Figure S2. The dependence of the sYFP fluorescence ratio *R* onto pH is shown. The E_{xr} (A) and E_{mr} (C) measured dependence of the two intensities F_1 and F_2 on pH and fits to Equation S1 and S2 are shown; experimental values (○,△); values of F_1 and F_2 scaled by a common factor to compensate for experimental variations of concentration with pH (▲,●). The E_{xr} (B) and E_{mr} (D) measured dependence of the ratio $R=F_1/F_2$ on pH and a fit to Equation 1 are shown. For each calibration, three different ROIs were analyzed. Details of the measurements can be found in the Experimental Section in the main text.

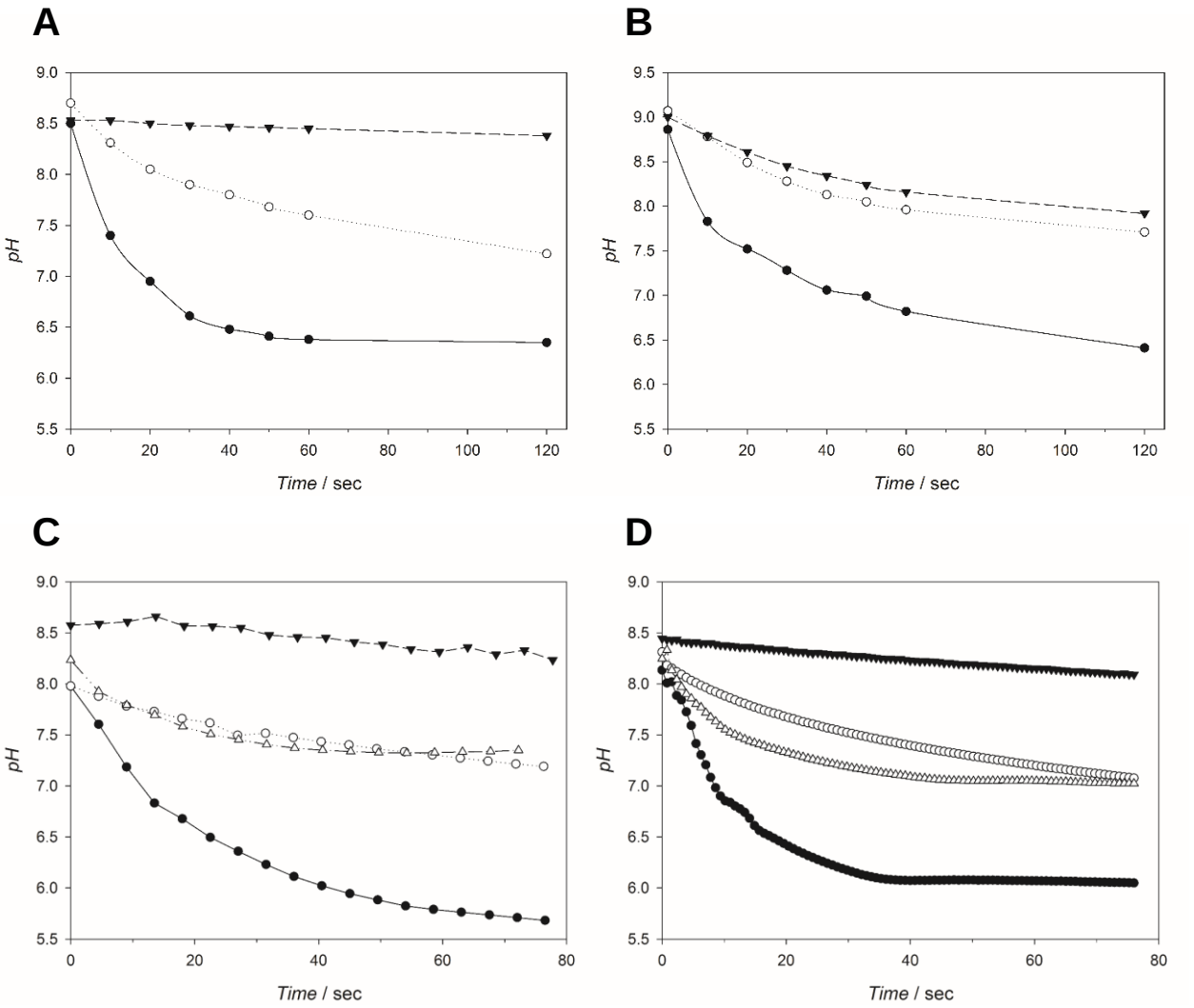

Figure S3. The pH time courses for the hydrolysis of 10 mM PenG catalyzed by soluble PGA are shown. The pH time course measured in a flask (100 mL) stirred at 300 rpm (A, B) or using soluble sYFP as a fluorescent pH sensor (C, D). (A) Times courses measured in 10 mM sodium phosphate buffer and an activity of 30 U_{PenG} mL^{-1} (●), 3 U_{PenG} mL^{-1} (○) and 0.06 U_{PenG} mL^{-1} (▼) are shown. (B) Times courses measured with an activity of 14.6 U_{PenG} mL^{-1} in 10 mM sodium phosphate buffer (●), 100 mM sodium phosphate buffer (○) and 200 mM sodium phosphate buffer (▼) are shown. E_{xr} (C) and E_{mr} (D) measured time courses in 10 mM sodium phosphate buffer (stagnant solution) with a activity of 30 U_{PenG} mL^{-1} (●), 3 U_{PenG} mL^{-1} (○) and 0.3 U_{PenG} mL^{-1} (▼) are shown. Every time course point corresponds to space-averaged pH within one ROI (whole field of view of suspension), each time course is exemplary shown for multiple experiments performed.

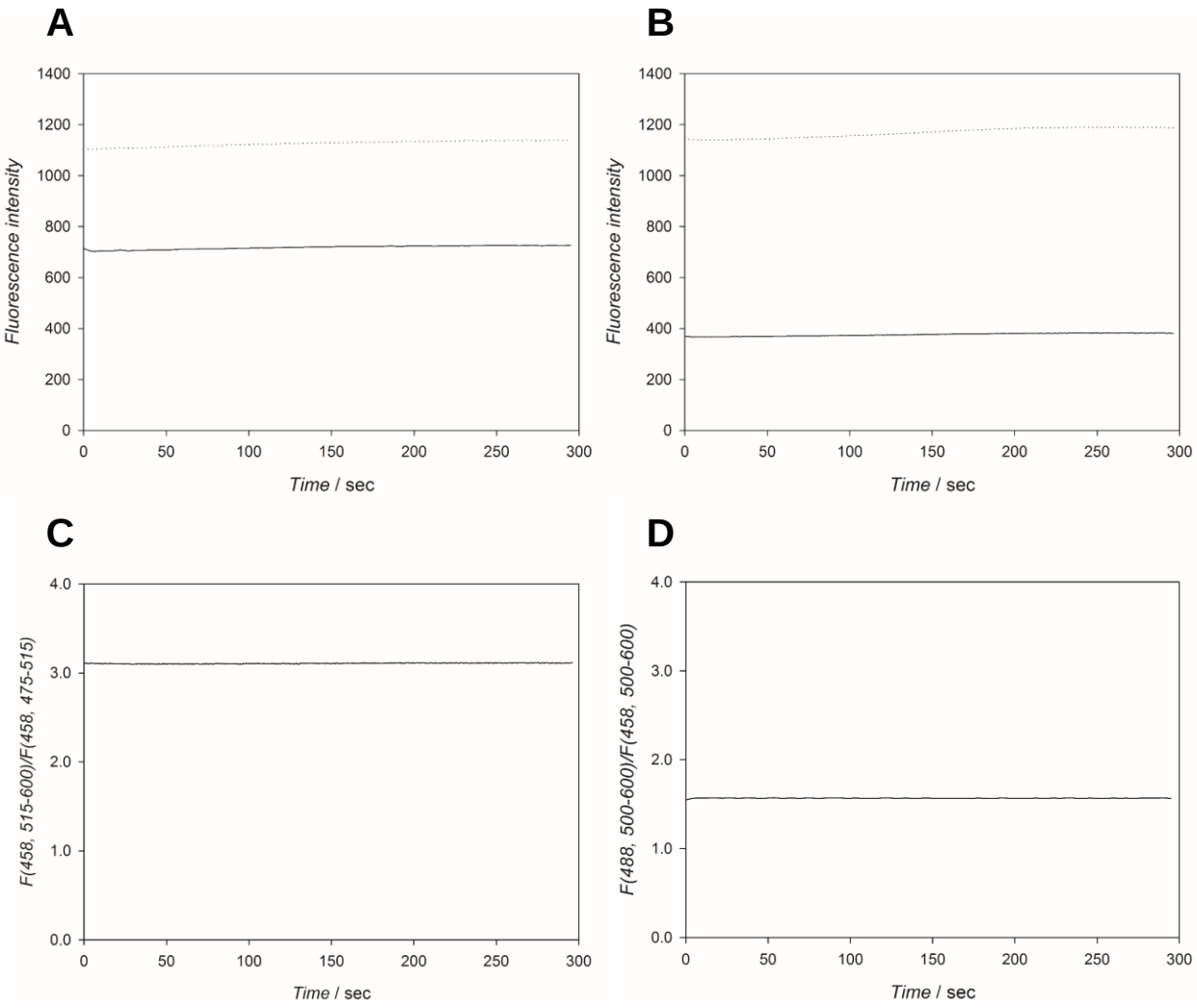

Figure S4. Photobleaching analysis of soluble sYFP during the timespan of a typical enzyme catalyzed reaction is shown. (A) Fluorescence intensity measured with the Ex_r setup: F(458, 500-600) (solid line), F(488, 500-600) (dotted line) and (B) ratiometric fluorescence signal. (C) Fluorescence intensity measured with the Em_r setup: F(458, 515-600) (dotted line), F(458, 475-515) (solid line) and (D) ratiometric fluorescence signal.

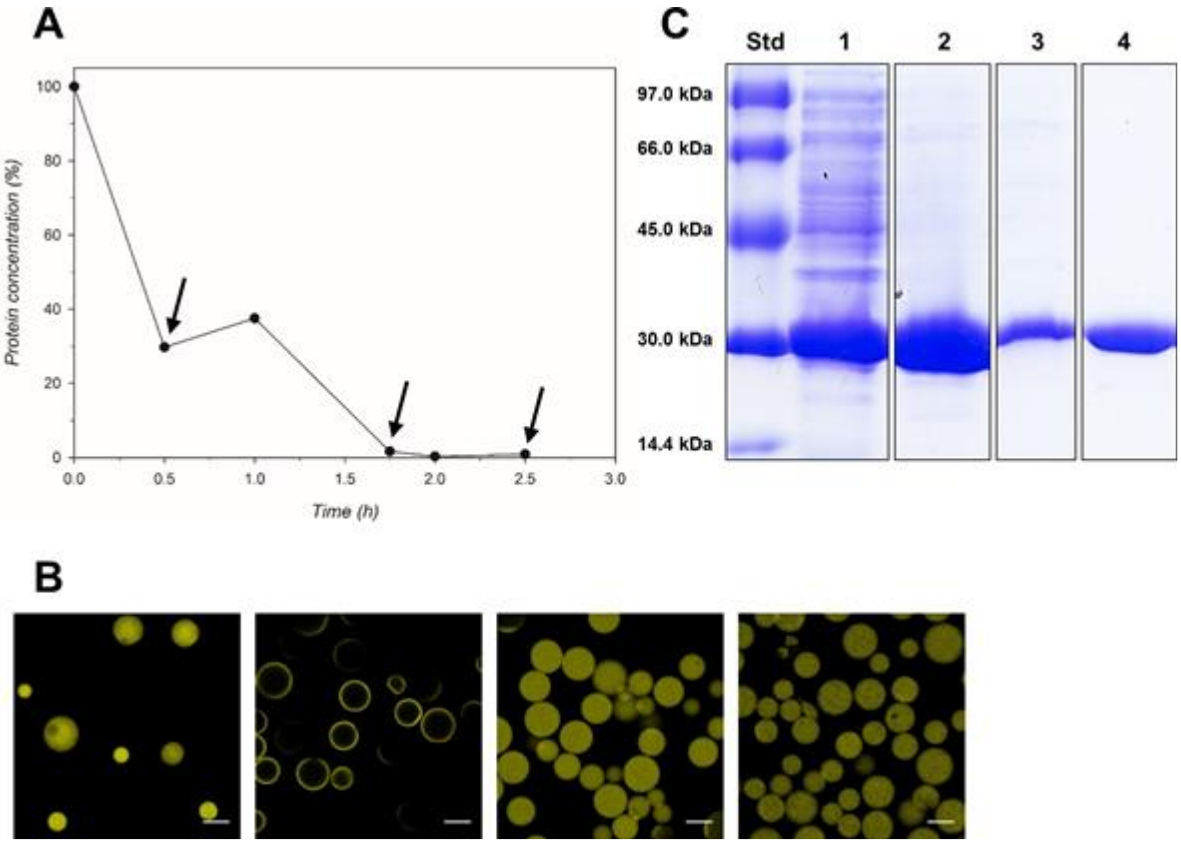

Figure S5. Immobilization of sYFP on Ag-Ni is shown. (A) Decrease of the sYFP protein concentration in supernatant during immobilization. The initial imidazole concentration (300 mM) was diluted stepwise by addition of fresh buffer (indicated by arrows) to a final concentration of 37.5 mM. The immobilizate was then incubated overnight. (B) Confocal images of sYFP distribution on Ag-Ni are shown. From left to right: serial dilution of 300 mM imidazole as shown in A, absence of imidazole, presence of 50 mM imidazole and 100 mM imidazole. The scale bar is 100 μm. (C) Coomassie stained 12% polyacrylamide gel showing the purification of sYFP is represented. (M) Size marker (Pharmacia LMW kit (14.4-97.0 kDa) (1) *E. coli* cell extract; (2) protein bound to Ag-Ni; (3) protein remaining after sodium phosphate buffer washes; (4) protein desorbed from the beads.

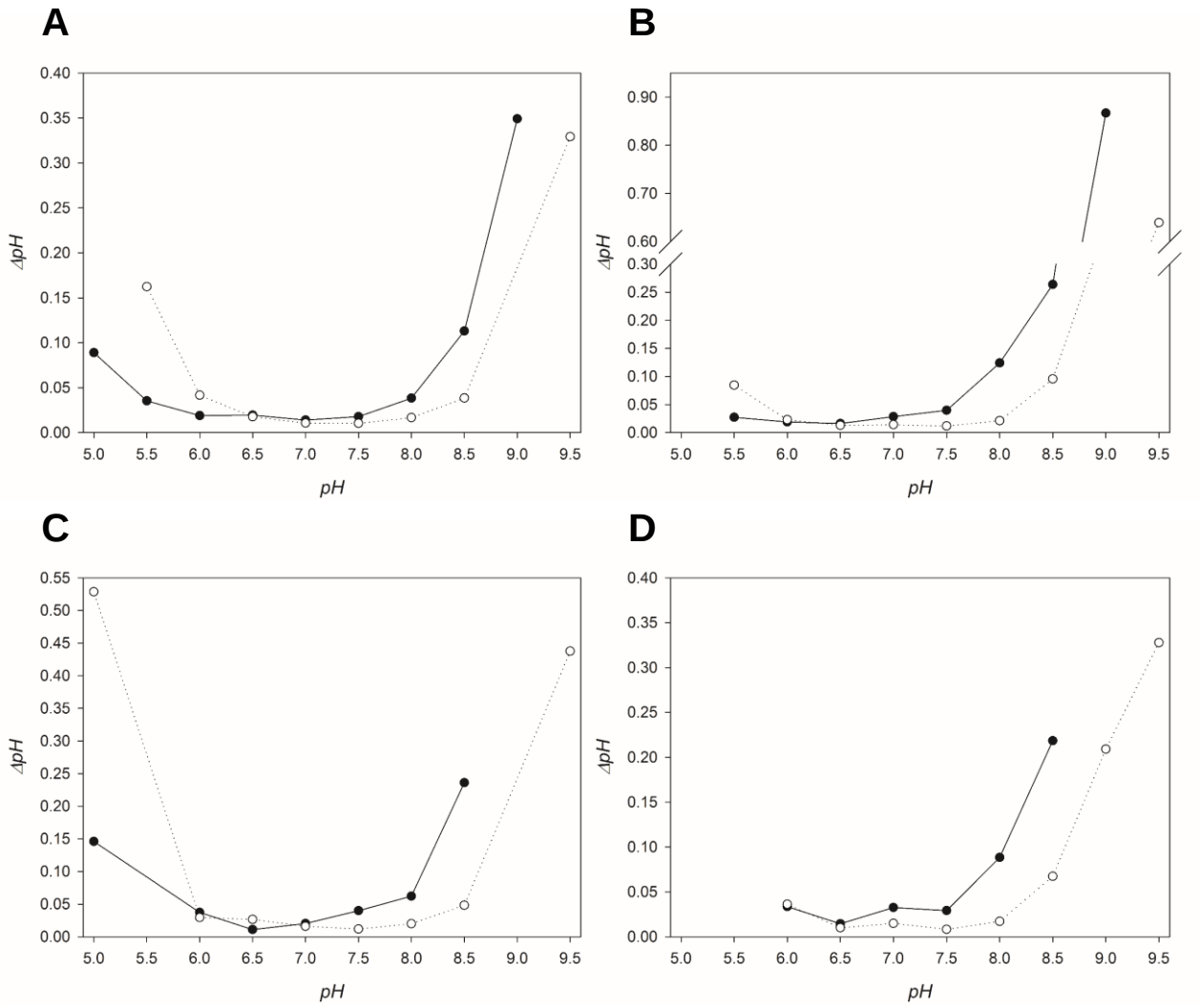

Figure S6. Uncertainty in the calculation of the pH at different pH values for the different materials used is shown. The values were calculated using Equation S6. The sYFP immobilized onto (A) Ag-Ni, (B) CPG-Ni, (C) Sep-Ni and (D) Ag-Gly is shown.

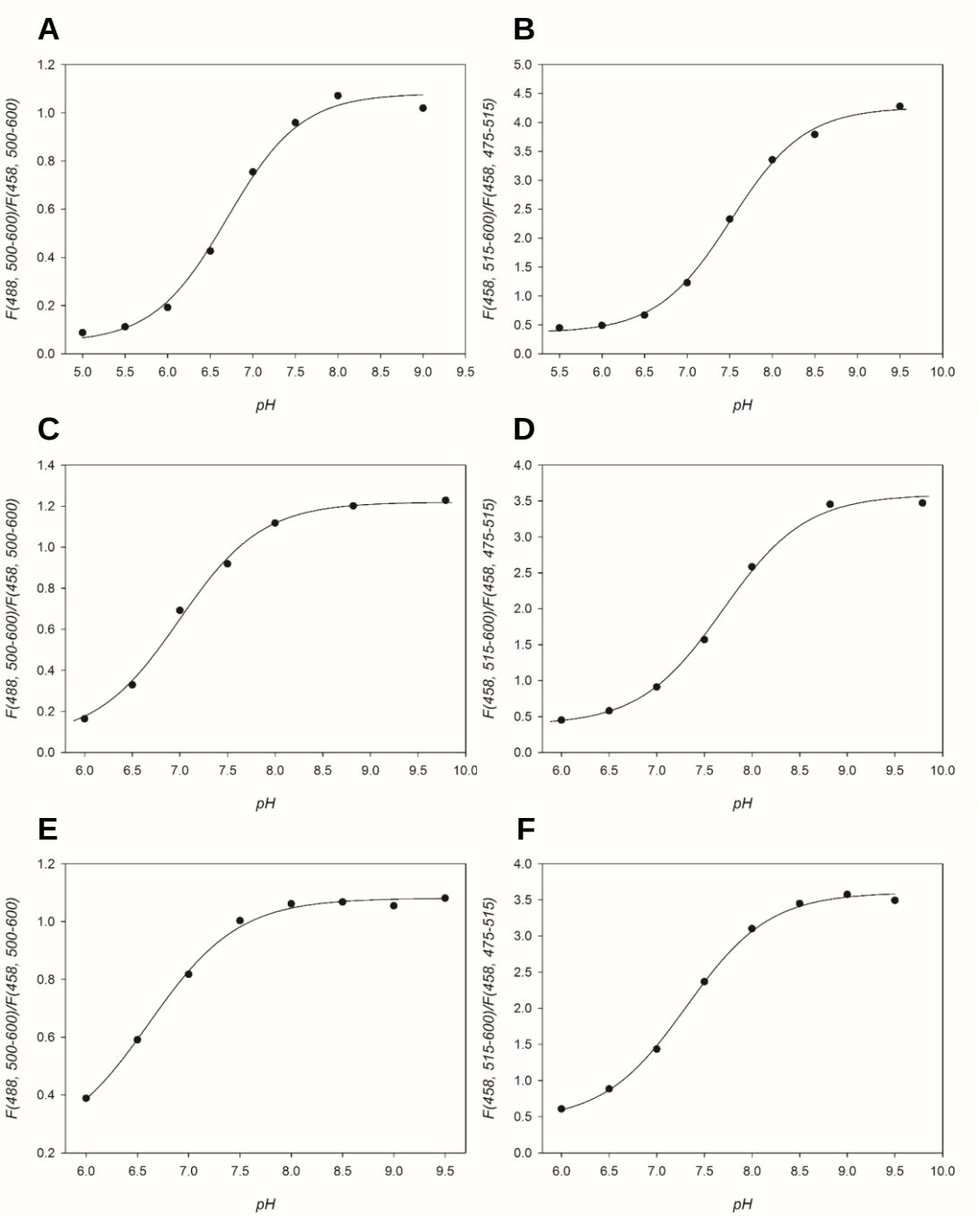

Figure S7. The pH response curves obtained for sYFP immobilized on different carrier materials is shown. All calibrations were fitted to Equation 4. Each point represents an average of five different ROIs. The panels show: Ex_r (A, C, E) and Em_r (B, D, F) calibration of sYFP-CPG-Ni (A, B), sYFP-Sep-Ni (C, D) and sYFP-Ag-Gly (E, F).

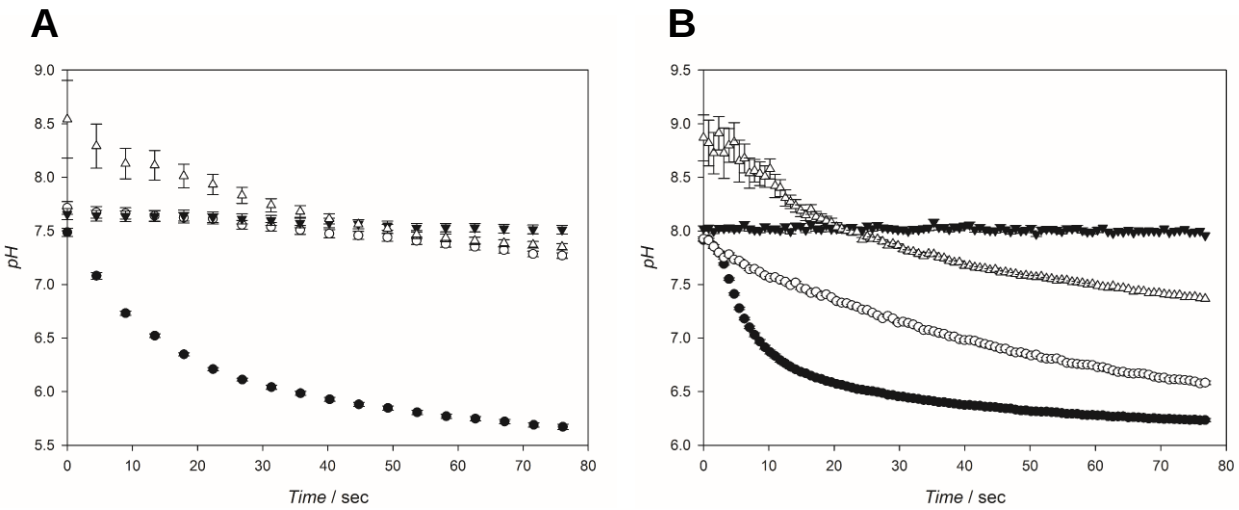

Figure S8. Analysis of the dynamic pH response of sYFP-CPG-Ni is shown. The pH decrease in 10 mM sodium phosphate buffer was measured by Ex_r (A) and Em_r (B) using a volumetric activity of 30 U_{PenG} mL^{-1} (●), 3 U_{PenG} mL^{-1} (○) and 0.3 U_{PenG} mL^{-1} (▼). Using 30 U_{PenG} mL^{-1} the reaction was also performed in 100 mM sodium phosphate buffer (△). Uncertainties of the pH determination calculated according to Equation S6 are shown with error bars. Every time course point corresponds to space-averaged pH within one ROI (one particle), each time course is exemplary shown for multiple experiments performed.

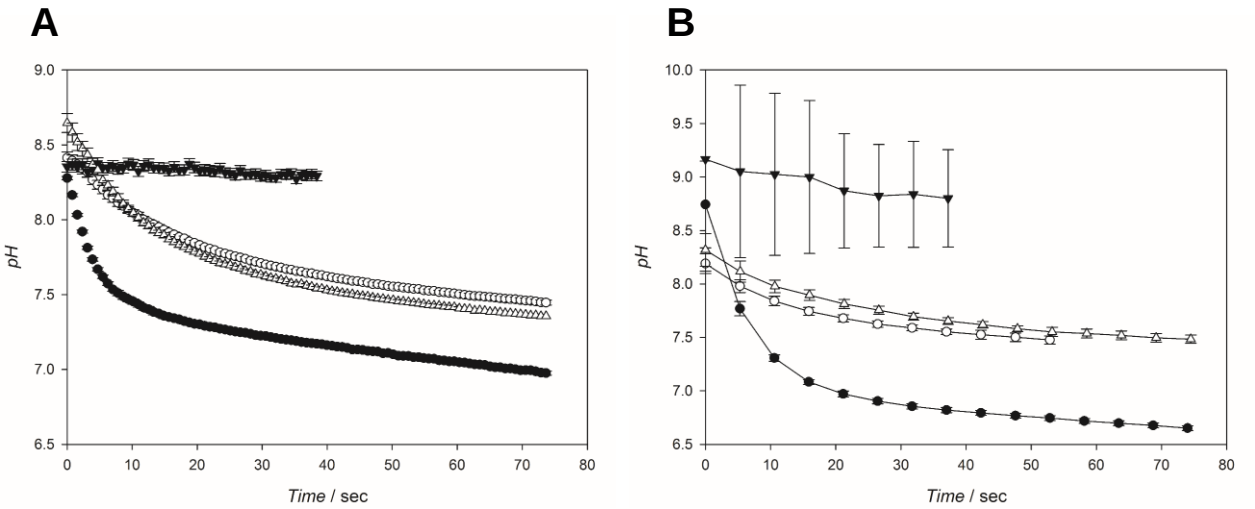

Figure S9. Analysis of the dynamic response of sYFP-Sep-Ni is shown. The pH decrease in 10 mM sodium phosphate buffer was measured by Ex_r (A) and Em_r (B) using an activity of 30 U_{PenG} mL^{-1} (●), 3 U_{PenG} mL^{-1} (○) and 0.3 U_{PenG} mL^{-1} (▼). Using 30 U_{PenG} mL^{-1} the reaction was also performed in 100 mM sodium phosphate buffer (△). Uncertainties of the pH determination calculated according to Equation S6 are shown with error bars. Every time course point corresponds to space-averaged pH within one ROI (one particle), each time course is exemplary shown for multiple experiments performed.

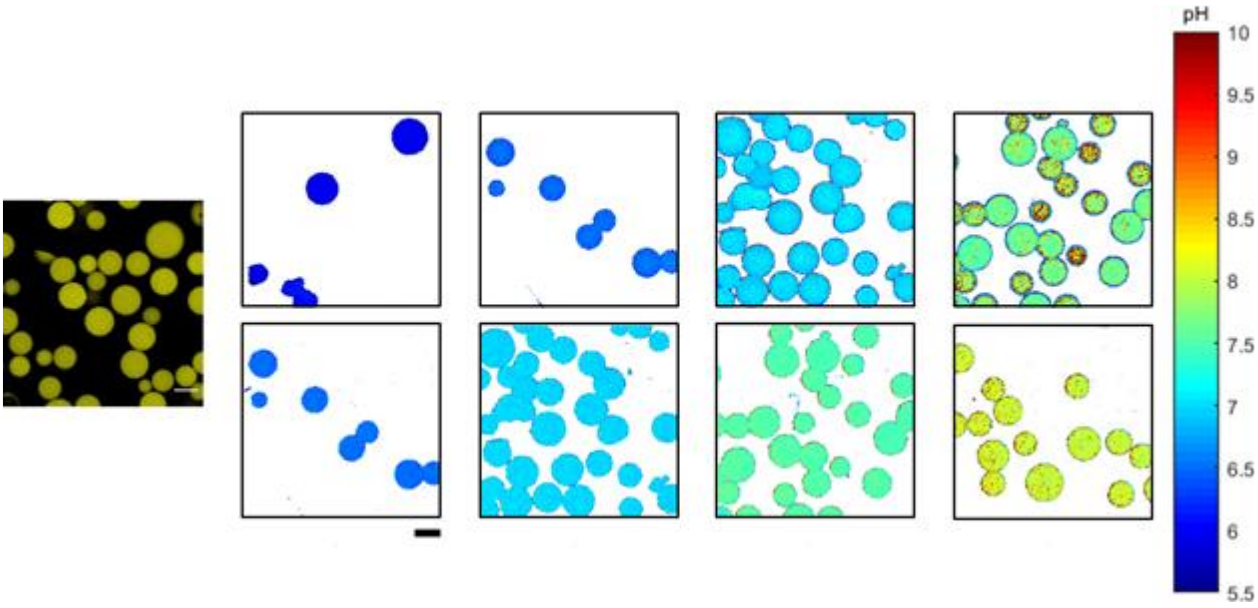

Figure S10. The pH response of sYFP-Ag-Gly is shown. A homogeneous sYFP distribution in particles obtained by stepwise dilution of 1 M ethanolamine is shown on the left. The shown pH maps correspond to the dynamic range of Ex_r (upper panel) and Em_r (lower panel) calibration. Scale bar is 100 micrometer.

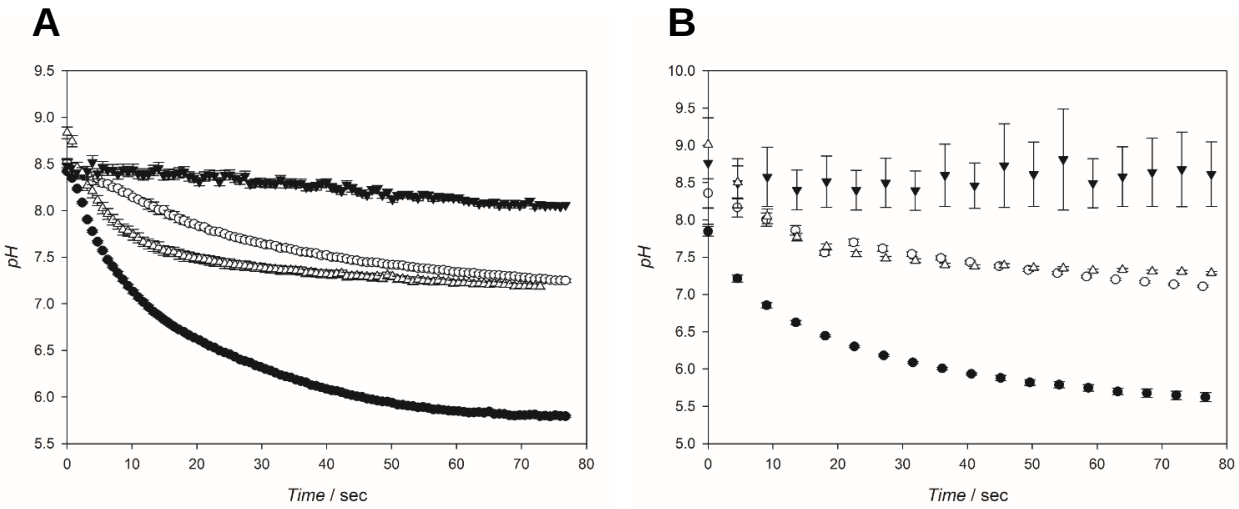

Figure S11. Analysis of the dynamic response of sYFP-Ag-Gly is shown. The pH decrease in 10 mM sodium phosphate buffer was measured by Ex_r (A) and Em_r (B) using an activity of 30 U_{PenG} mL^{-1} (●), 3 U_{PenG} mL^{-1} (○) and 0.3 U_{PenG} mL^{-1} (▼). Using 30 U_{PenG} mL^{-1} the reaction was also performed in 100 mM sodium phosphate buffer (△). Uncertainties of the pH determination calculated according to Equation S6 are shown with error bars. Every time course point corresponds to space-averaged pH within one ROI (one particle), each time course is exemplary shown for multiple experiments performed.

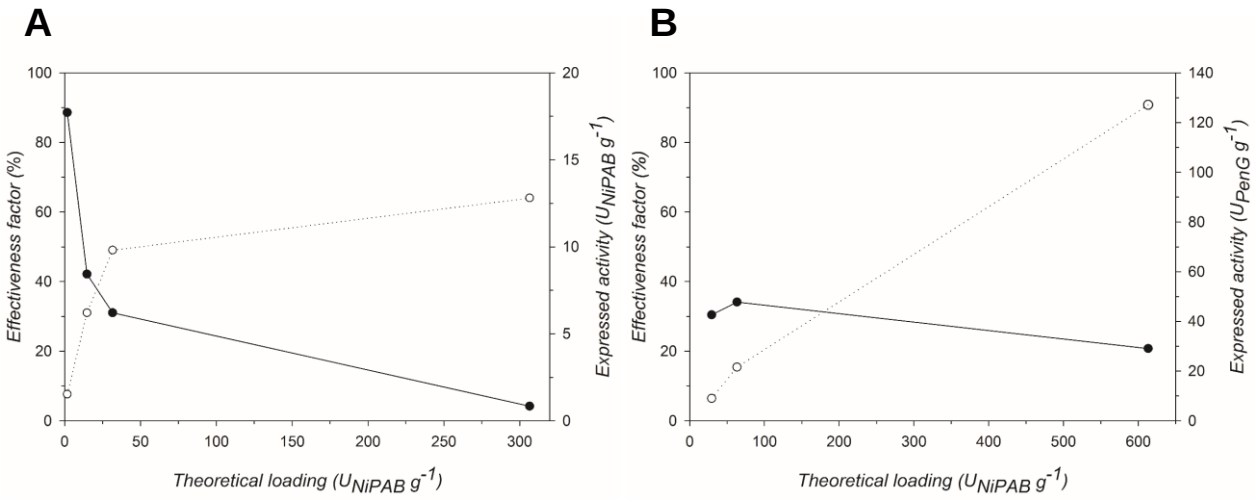

Figure S12. The dependencies of the effectiveness factor (●) and the expressed activity (○) on the theoretically loaded activity of PGA immobilized onto Ag-Ni-Gly are shown. The activities were determined with (A) NiPAB or (B) PenG as the substrate. The effectiveness factor is the ratio of the observed to the theoretically immobilized enzyme activity. The theoretical activity is determined from a balance of activity measurable in the supernatant before and at the end of immobilization.

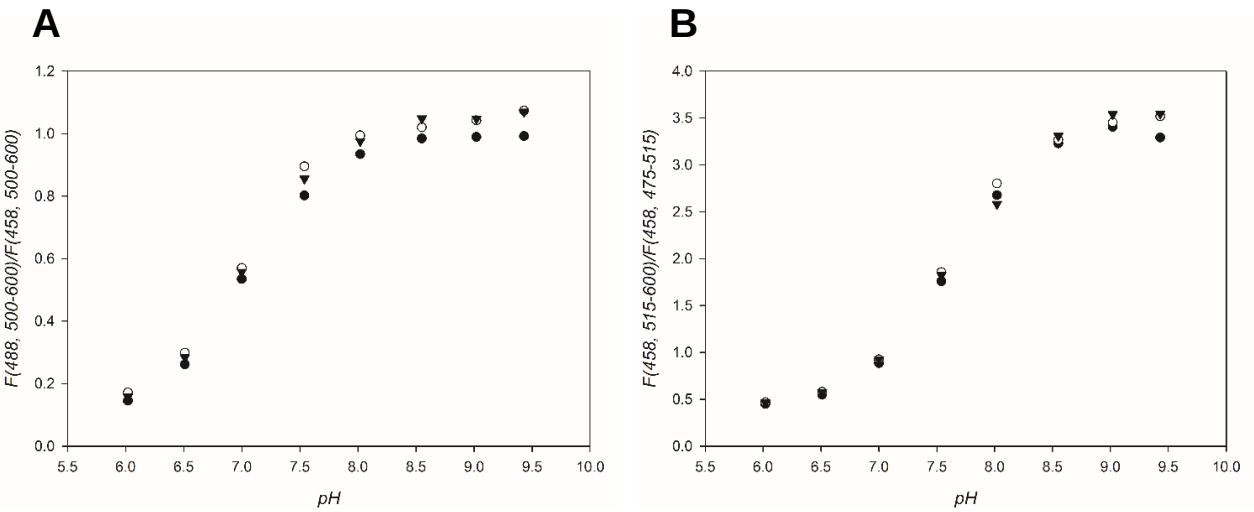

Figure S13. The dependence of the measured fluorescence ratio on pH is shown. Panel (A) shows the excitation ratiometric calibration while panel (B) shows the emission ratiometric calibration, each for a sYFP-PGA-Ag-Ni-Gly coimmobilizate. For each calibration, three enzyme loadings were analyzed, 805 U_{PenG} g^{-1} (●), 135 U U_{PenG} g^{-1} (○) and 27 U U_{PenG} g^{-1} (▼).

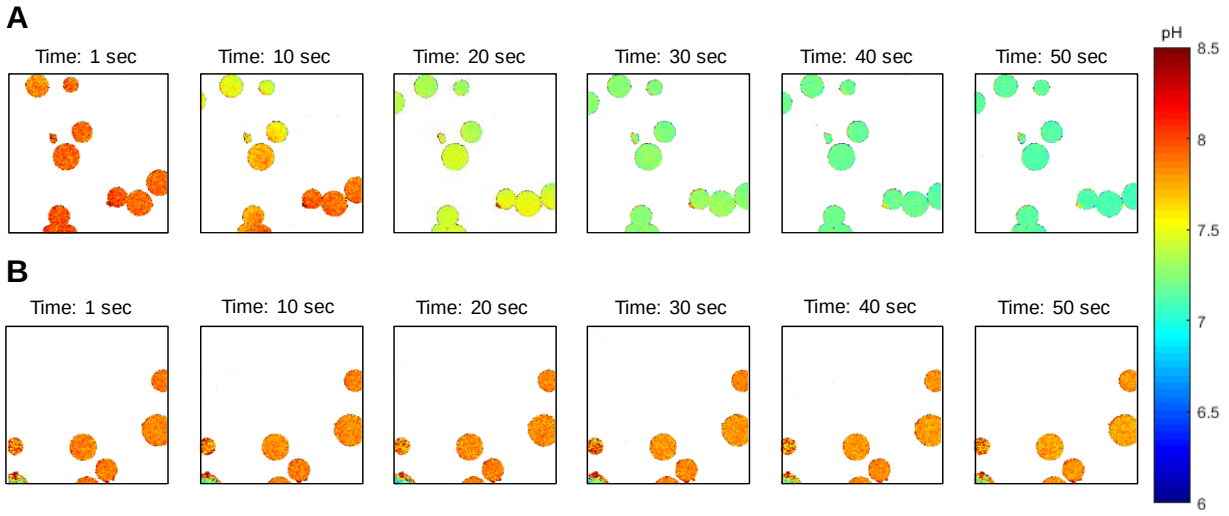

Figure S14. The spatiotemporal mapping of the intraparticle pH using sYFP immobilized onto Ag-Ni is shown. Soluble PGA was used to carry out the enzymatic reaction. Panel (A) shows a reaction using 3 U_{PenG} mL^{-1}.(VideoS1). Panel (B) shows a reaction, in which an enzyme activity of 0.3 U_{PenG} mL^{-1} was used (Video S2). The range of amount of free PGA used covers all the experiments shown in Figure 4 and 5, in terms of equivalent volumetric activity of acylase were used.

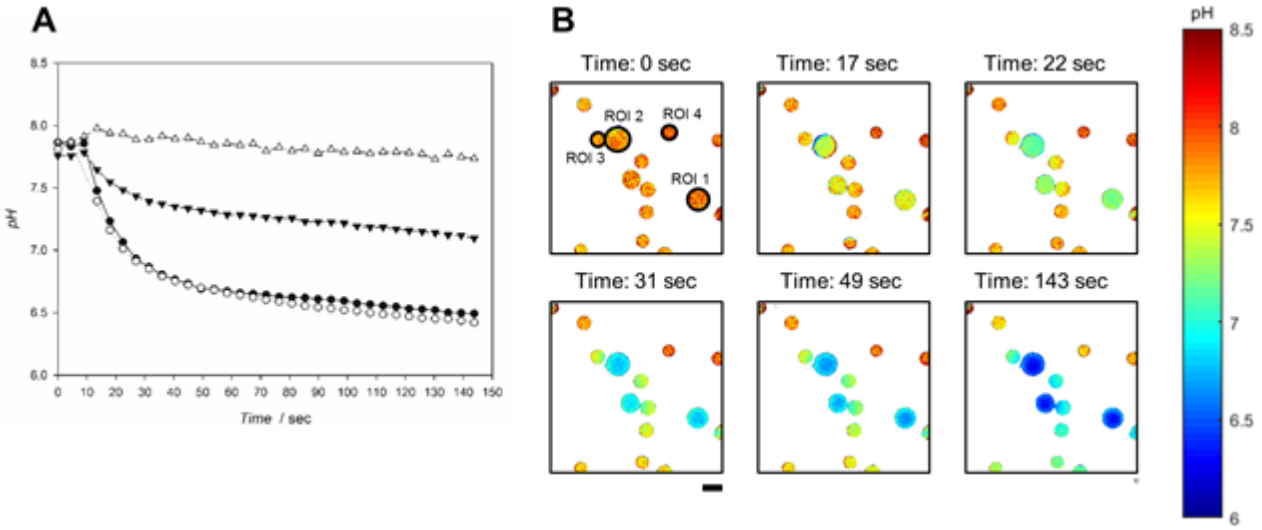

Figure S15. The spatiotemporal mapping of the intraparticle pH for a sYFP-PGA-coimmobilizate on Ag-Ni-Gly measured with Ex_r is shown. The PGA loading was 805 U_{PenG} g^{-1} of carrier. Reactions were performed using 20 mM PenG as substrate in 10 mM SBP. (**A**) The space averaged pH time courses of 4 different ROIs highlighted with a black circle in B are shown. ROI 1 and 2 are bulk particles, ROI 3 and 4 are catalyst particles. ROI 1 (●) and ROI 2 (○) ROI 3 (▼) and ROI 4 (△) (**B**) pH maps of different time points during sYFP-PGA-coimmobilizate reaction are shown. The scale bar is 100 micrometer.

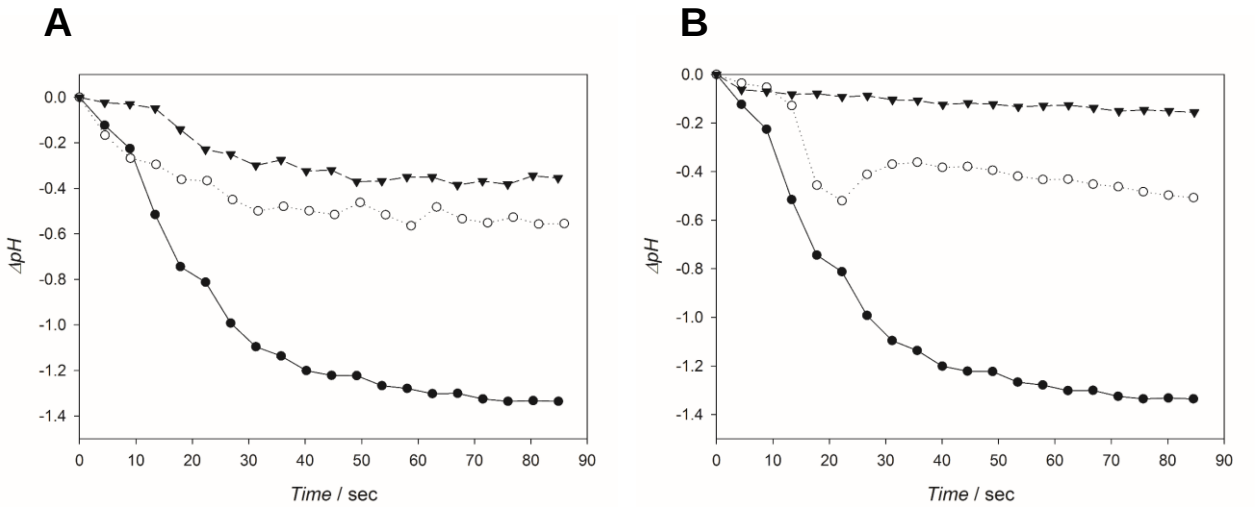

Figure S16. The ΔpH time courses for PenG hydrolysis by a sYFP-PGA-coimmobilizate on Ag-Ni-Gly measured with Ex_r are shown. The ΔpH was calculated as the difference between the spaced-averaged pH within sYFP-PGA-coimmobilizate and the bulk solution. Panel (A) shows the dependence of the ΔpH time courses on buffer variation, testing sodium phosphate concentrations of 10 mM (●), 100 mM (○) and 200 mM (▼). The PGA loading was 805 U_{PenG} g^{-1} of carrier. Reactions were performed using 20 mM PenG as substrate. Panel (B) shows the dependence of the ΔpH time courses on different concentrations of immobilized PGA used, starting at pH 8.0. The enzyme loading was 805 U_{PenG} g^{-1} (●), 130 U_{PenG} g^{-1} (○) and 27 U_{PenG} g^{-1} (▼).

Table S1. Characterization of a sYFP-PGA-coimmobilizate as ratiometric pH sensor

Ratiometric method		Excitation						Emission					
Sample		Enzyme particle			Control particle			Enzyme particle			Control particle		
Enzymatic Loading	Parameter	R_0	pK'	R_f	R_0	pK'	R_f	R_0	pK'	R_f	R_0	pK'	R_f
805 IU_{PenG} g^{-1}	Coefficient	0.04	6.98	26.93	0.04	7.02	28.89	0.31	7.59	11.17	0.31	7.62	11.55
	Std Error	0.02	0.03	12.77	0.04	0.07	32.03	0.07	0.05	2.55	0.08	0.05	2.72
135 IU_{PenG} g^{-1}	Coefficient	0.05	6.95	21.42	0.05	6.96	21.16	0.33	7.58	10.92	0.31	7.59	11.99
	Std Error	0.03	0.06	14.82	0.05	0.08	20.26	0.05	0.03	1.61	0.07	0.05	2.78
27 IU_{PenG} g^{-1}	Coefficient	0.05	7.00	20.49	0.05	7.02	22.44	0.37	7.66	9.82	0.33	7.61	11.59
	Std Error	0.02	0.03	6.44	0.03	0.04	11.01	0.04	0.03	1.03	0.07	0.05	2.49

Parameters are from nonlinear fits of Equation 1 to the pH response curves of sYFP attached to the solid material

Supporting references

(1) Mateo, C.; Fernandez-Lorente, G.; Rocha-Martin, J.; Bolivar, J. M.; Guisan, J. M. Oriented Covalent Immobilization of Enzymes on Heterofunctional-Glyoxyl Supports. In *Immobilization of Enzymes and Cells*; Guisan, J. M., Ed.; Humana Press: Totowa, NJ, 2013; Vol. 1051, pp 73–88.

(2) Bernal, C.; Sierra, L.; Mesa, M. Improvement of Thermal Stability of β-Galactosidase from *Bacillus Circulans* by Multipoint Covalent Immobilization in Hierarchical Macro-Mesoporous Silica. *J. Mol. Catal. B Enzym.* **2012**, *84*, 166–172.

(3) Mateo, C.; Grazu, V.; Guisan, J. M. Immobilization of Enzymes on Monofunctional and Heterofunctional Epoxy-Activated Supports. In *Immobilization of Enzymes and Cells*; Guisan, J. M., Ed.; Humana Press: Totowa, NJ, 2013; Vol. 1051, pp 43–57.

(4) Valencia, P.; Wilson, L.; Aguirre, C.; Illanes, A. Evaluation of the Incidence of Diffusional Restrictions on the Enzymatic Reactions of Hydrolysis of Penicillin G and Synthesis of Cephalexin. *Enzyme Microb. Technol.* **2010**, *47* (6), 268–276.

(5) Alvaro, G.; Fernandez-Lafuente, R.; Blanco, R. M.; Guisán, J. M. Immobilization-Stabilization of Penicillin G Acylase from *Escherichia coli*. *Appl. Biochem. Biotechnol.* **1990**, *26* (2), 181–195.

(6) Jonathon Shlens. A Tutorial on Principal Component Analysis. *ArXiv14041100 CsLG*.